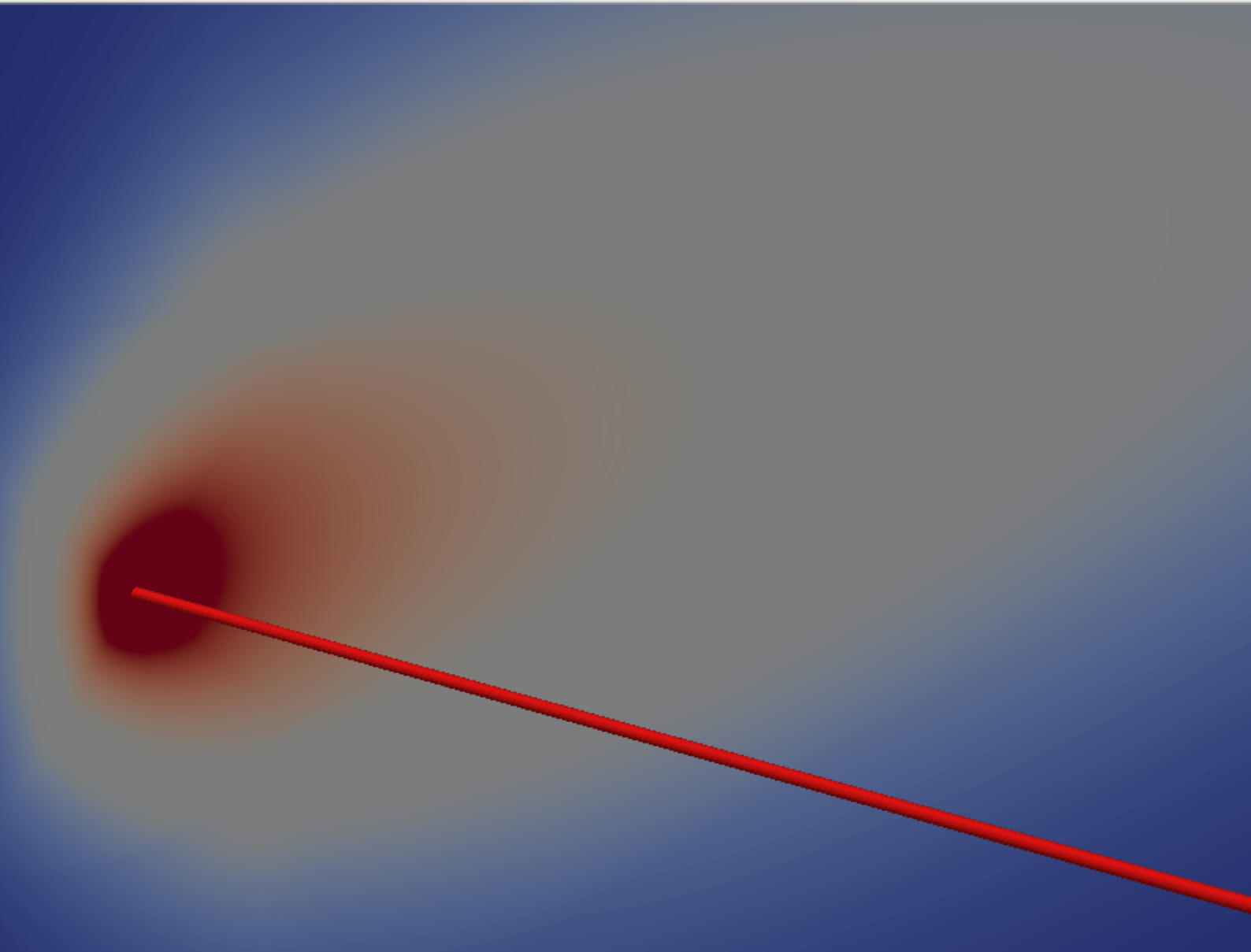
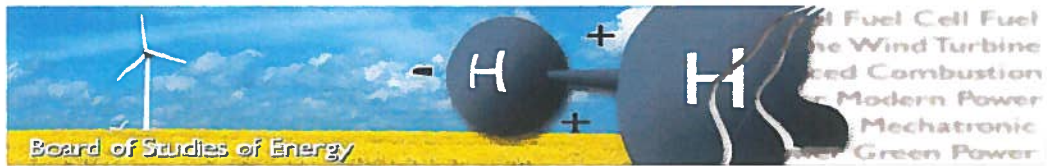


CFD analysis to determine the local Nusselt number over a heated micro wire in multicomponent flow



AALBORG UNIVERSITY
DENMARK

Gerrit Nils Werner
Master's thesis, June 2016
Thermal Energy and Process Engineering



Title: CFD analysis to determine the local Nusselt number over a heated micro wire in multicomponent flow
Semester: 10th, spring semester 2016
Semester theme: Master's thesis
Project period: 01.02.2016 to 01.06.2016
ECTS: 30
Supervisors: Torsten Berning
Project group: TEPE4-1003

Gerrit Nils Werner

SYNOPSIS:

In order to gain knowledge about the influence of a hot wire anemometer to its surrounding and to validate experimental results from a laboratory, a CFD model is developed which contains a pipe and the wire. The wire is placed in the center of the pipe. This model is capable of running with different gas compositions and humidifications, only dependent on temperature. To achieve a fast meshing and simulating process, the model is two dimensional. This model showed that at low velocities heat diffuses upstream and that the outlet temperature is dependent on the flow velocity. A higher velocity results in a lower temperature. Furthermore natural convection can be neglected in the presented cases. The coefficients for the Nusselt number correlation were found similar to the coefficients from the laboratory, but containing some deviations that might be caused by the way of evaluating. Furthermore a three dimensional model is build to estimate the deviation between the two dimensional and three dimensional model. It was found that in the two dimensional model more heat per wire length is transferred to the fluid.

Copies: 3
Pages, total: 68
Appendixes: 4

By signing this document, I confirm that the report does not include plagiarism.

Preface

This thesis was composed between February 2016 and June 2016 as a Master's thesis during the 10th semester of the study program Thermal Energy and Process Engineering at Aalborg University. The aim of this project is to model a hot wire anemometer used to measure the humidification of a hydrogen stream of a fuel cell to guaranty a precise water management.

The report presupposes thereby a level of knowledge about fundamental thermodynamics, fluid dynamics and computational fluid dynamics. Besides it may be helpful to have a certain knowledge about OpenFOAM, paraFoam and MATLAB as these three tools were used to run the simulation and handle the data afterwards.

I would like to thank my supervisor Torsten Berning for his guidance and support during the semester. Furthermore I would like to thank Saher Al Shakhshir for the discussions and the laboratory support.

Instructions:

This report conforms to the standard of scientific citing. Therefore the Harvard citation method was used, where sources are listed in the text as [Surname, year]. This refers to the bibliography, which can be found at the end of the report, before the Appendix. The sources are listed alphabetically. Books are listed starting with the author, year, title, edition and publisher, whereas Websites are listed with author, title, date and URL.

Equations, tables and figures are numbered related to the current chapter and in order of appearance.

Nomenclature

Abbreviations

Abbreviation	Explanation
MCFC	Molten carbonate fuel cell
PAFC	Phosphoric acid fuel cells
PEMFC	Proton Exchange Membrane Fuel Cells
SOFC	Solid oxide fuel cell
O	Oxygen
H	Hydrogen
e^-	Electron
z	Number of moles
S	Stoichiometric ratio
Nu	Nusselt number
Pe	Peclet number
Pr	Prantl number
Gr	Grashof number
x_i	Molar fraction of species i
y_i	Mass fraction of species i

Symbol list

Symbol	Explanation	Unit
A	Area	[m ²]
c_p	Specific heat capacity	[J kg ⁻¹ K ⁻¹]
D	Diameter	[m]
E	Volt	[V]
F	Faraday's constant	[96485 C mol ⁻¹]
g	Gravity	[m ² s ⁻¹]
h	Convection coefficient	[W m ⁻² K ⁻¹]
I	Current	[A]
k	Thermal conductivity	[W m ⁻¹ K ⁻¹]
L	Length	[m]
\dot{m}	Mass flow	[kg s ⁻¹]
n	Amount of substance	[mol]
\dot{Q}	Heat flow	[W]
R	Resistance	[Ω]
r_d	Net drag coefficient	[-]
T	Temperature	[K]
t	Time	[s]
u	Velocity	[m s ⁻¹]
β	Expansion coefficient	[K ⁻¹]
ν	Viscosity	[m ² s ⁻¹]

Symbol	Explanation	Unit
τ	Stress tensor	[N m ⁻²]
ϕ	Property or dissipation function	[-]

Commonly used subscripts

Symbol	Explanation
<i>charac</i>	Characteristic
<i>crit</i>	Critical
<i>film</i>	Film temperature
<i>g</i>	Gas
<i>P</i>	Pipe
<i>w</i>	Wire

Table of contents

Chapter 1 Introduction	3
1.1 Proton Exchange Membrane Fuel Cell	3
1.1.1 Operating Principle	3
1.1.2 Water generation and transport in a fuel cell	4
1.2 Hot wire anemometry	6
Chapter 2 Computational model	11
2.1 Governing Equations - General approach	11
2.2 Governing Equations - Boussinesq approximation	12
2.3 Critical Reynolds number	13
2.4 Mixture properties	13
2.4.1 Temperature dependent fluid properties	14
Chapter 3 Analytical considerations	17
3.1 Hagen-Poiseuille flow in a pipe	17
3.2 Hagen-Poiseuille flow between two not moving parallel plates	19
Chapter 4 Model description	21
Chapter 5 2D model	23
5.1 Geometric description of the two dimensional model	23
5.2 Meshing of the model	24
5.3 Boundary definitions	25
5.4 Interpretation of the two dimensional model	26
5.5 Grid independence study	26
5.6 CFD simulation start cases	29
5.7 Influence of the hot wire on the surrounding	29
5.8 Nusselt number results	36
5.8.1 Method of evaluation the Nusselt number	36
5.8.2 Dry hydrogen	38
5.8.3 Humidified hydrogen	40
5.8.4 Dry hydrogen - Local Nusselt number	42
5.9 Different wire diameter	44
Chapter 6 3D model	47
6.1 Model setup	47
6.2 Results	49
Chapter 7 Conclusion	51
7.1 Influence on the surrounding	51
7.2 Nusselt number and estimation of the coefficients	51
Chapter 8 Future work	53

Bibliography	55
Appendix A Material properties	59
A.1 Raw data	59
A.1.1 Hydrogen	59
A.1.2 Water vapor	59
A.2 Functions	59
A.2.1 H2 0% RH	60
A.2.2 H2 20% RH	60
A.2.3 H2 40% RH	60
A.2.4 H2 60% RH	60
A.2.5 H2 80% RH	61
A.2.6 H2 100% RH	61
Appendix B Blocking plan	63
Appendix C Guideline for the enclosure	65
C.1 Content	65
C.2 How to run a case	66
Appendix D Post processing tools	67

Study objective

Due to the increasing demand for a reduction of the carbon footprint, alternative energy supplies are needed. Fuel cells are one technology and they are in direct competition to other techniques like e.g gas turbines and combustion engines, as well as batteries [Z.Sharaf and F.Orhan, 2014]. Especially in the car industry proton exchange membrane fuel cells (PEMFC) are of high importance, due to their compactness, low start-up time and cost compared to solid oxide fuel cells. Furthermore these fuel cells do not exhaust carbon based gases nor particles like combustion engines and have a higher range than electric cars based on batteries.

The operation of PEMFCs is highly depended on the water management inside the fuel cell: The electrodes and the membrane need to be humidified sufficiently to enable good operating conditions, but shall not be flooded either. To gain knowledge about the water balance, it is measured dependent on several parameters at different loads. A variety of methods is used to obtain information about the water management, but only hot wire anemometry can be used ad-hoc. Such a hot wire is placed in the exhaust pipe of the anode while measuring the voltage signal through it, which is dependent on the heat transferred from the wire to the gas stream. The heat transfer is thereby dependent on the gas composition and humidification.

The aim of this study is to validate results from the laboratory of the hot wire and gain detailed knowledge about the influence of the hot wire on the surrounding. Especially Nusselt numbers of different cases are of high interest, as the results of this study shall validate coefficients for the power-law. Besides the overall Nusselt number, local Nusselt numbers shall be used, to investigate the heat transfer distribution around the wire.

Therefore a model needs to be set up that contains the wire and the pipe carrying the gas. It has to be capable of running with different gas compositions, including heat transfer and the effects of gravity, for the case that natural convection plays a role.

Introduction

1

1.1 Proton Exchange Membrane Fuel Cell

Fuel cells are systems that convert chemical potential energy into electricity and heat by running an electrochemical reaction. Therefore the fuel cell uses an anode and a cathode where the reactions take place and a membrane to separate them while allowing transport of ions. The different types of fuel cells are categorized according to their electrolyte material [Z.Sharaf and F.Orhan, 2014].

Common fuel cells are:

- Proton Exchange Membrane Fuel Cells (PEMFC)
- Phosphoric acid fuel cells (PAFC)
- High-temperature fuel cells such as Solid oxide fuel cell (SOFC) or Molten carbonate fuel cell (MCFC)

This study considers only PEMFC fuel cells using hydrogen as fuel and air as the oxidant. Both streams may contain a certain amount of humidity.

PEMFC usually operate at temperatures between 50°C and 80°C, have a fuel efficiency of converting chemical to electrical energy of 45-60% and have a relatively low capital cost compared to other fuel cell systems [Peighambardoust et al., 2010].

Figure 1.1 shows the working principle of a PEMFC.

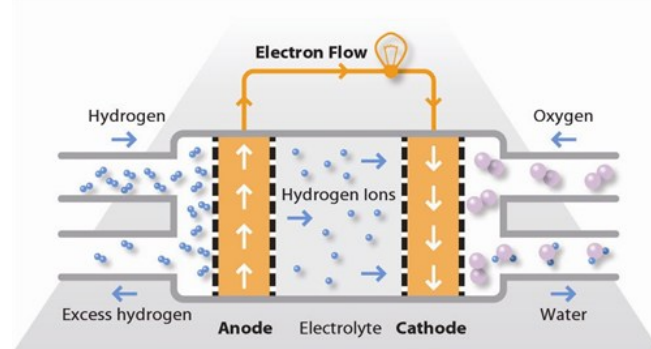


Figure 1.1. Set up of a PEMFC [FuelCellToday].

The principle of such a fuel cell is explained briefly in the following, based on Figure 1.1.

1.1.1 Operating Principle

Cathode

The cathode is made out of a porous material, which is covered with a catalyst. This catalyst layer often is platinum [Z.Sharaf and F.Orhan, 2014]. The incoming oxygen

reacts with protons and electrons to water molecules. Protons and electrons are a result of the anode reaction. The electrons migrated through an external circuit and the protons through the membrane. As often air is used to supply the cathode with oxygen, the excess stream is humidified air.

The reaction at the cathode is thereby:



Anode

Like the cathode, the anode is produced out of catalyst covered porous material. Incoming hydrogen molecules are split into protons (H^+) and electrons (e^-).

The anode reaction is:



Although the incoming stream is usually hydrogen from a pressurized storage, a small excess stream has to leave the anode again. This can be a mixture of hydrogen, water and small amount of nitrogen in some cases.

Overall

Summarizing the reaction from the anode and the cathode yields to the overall reaction:



From the overall Equation 1.3 it can be seen, that besides an electrical potential, water is a product of the reaction.

Membrane

The membrane is usually a polymer electrolyte membrane, which has to allow the transport of ions while disallowing electrons to pass to prevent a short cut. The electrons have to run through an external circuit, where a consumer can use the power.

Besides the protons, small amounts of nitrogen and a specific amount of water might diffuse through the membrane as well [Berning, 2013].

Besides problems with a hydrogen infrastructure or the cost of fuel cell systems, a big challenge nowadays is still the water management inside the fuel cell. This is dependent on the amount of water carried into the system and on the production rate due to the load. A bad water management can lower the efficiency or even cause permanent damage on the membrane. To prevent this, different technologies like a recirculation of gases or a direct water injection can be used to achieve a good water management [Abid and Masoud, 2013].

1.1.2 Water generation and transport in a fuel cell

The performance of a fuel cell can depend on the water balance. Due to the production of water at the cathode, it can be flooded in the worst case. On the other hand, the

anode can dry in worst case and thereby lower the load of the system. Furthermore the membrane shall be as humidified as possible to reduce ohmic losses [Hayre et al., 2006]. The water balance is dependent on the water that is transported into the fuel cell and on the load of a fuel cell, which can be related to the current. Using Faraday's law, the molar flow of the gas species into the anode and cathode can be calculated.

$$I \cdot t = n \cdot z \cdot F \quad \Leftrightarrow \quad \dot{n} = \frac{n}{t} = \frac{I}{z \cdot F} \quad (1.4)$$

Abbreviation	Explanation	Unit
I	Current	A
t	Time	s
n	Amount of substance	mol
z	Number of moles	-
F	Faraday's constant	96485 C mol ⁻¹
r	Volume / molar fraction	-
S	Stoichiometric ratio	-

Table 1.1. Faraday's law - Abbreviations.

Equation 1.4 can be reformulated in terms of molar flow of fuel:

$$\dot{n}_{fuel} = \frac{I \cdot S_{H_2}}{2 \cdot F \cdot r_{H_2}} \quad (1.5)$$

and oxidant:

$$\dot{n}_{oxidant} = \frac{I \cdot S_{O_2}}{4 \cdot F \cdot r_{O_2}} \quad (1.6)$$

If the compositions of the incoming gases are known, the flow of water entering the fuel cell can be calculated with Equation 1.5 and Equation 1.6 dependent on the load. It may be noticed, that the equations are set up for only one fuel cell. The outgoing molar flows of water are based on the incoming flows, the production rate and the diffusion from cathode to anode [Z.Sharaf and F.Orhan, 2014].

The molar flow of water leaving the cathode is calculated based on the following equation:

$$(\dot{n}_{H_2O})_{oxidant,out} = (\dot{n}_{H_2O})_{oxidant,in} + (\dot{n}_{H_2O})_{gen} + (\dot{n}_{H_2O})_{crossover} \quad (1.7)$$

Equation 1.7 sums up the molar flows based on the incoming water from the oxidant gas stream ($(\dot{n}_{H_2O})_{oxidant,in}$), the water generation due to the reaction itself ($(\dot{n}_{H_2O})_{gen}$) and internal water migration from the cathode to the anode ($(\dot{n}_{H_2O})_{crossover}$).

Corresponding to the cathode, the outgoing molar flow of water at the anode is:

$$(\dot{n}_{H_2O})_{fuel,out} = (\dot{n}_{H_2O})_{fuel,in} - (\dot{n}_{H_2O})_{crossover} \quad (1.8)$$

Inside the fuel cell a crossover of water through the membrane occurs due to different mechanisms. Commonly known ones are electro-osmotic drag, which results in a flow from

the anode to the cathode and back diffusion, which results in a flow from the cathode to the anode [Z.Sharaf and F.Orhan, 2014].

Electro-osmotic drag is caused by the transport of protons from the anode to the cathode, whereas back diffusion is caused by a difference in water concentration between anode and cathode [Jansen and Overvelde, 2001]. The crossover of water results in the so called net drag [Jansen and Overvelde, 2001].

The net drag coefficient based on the anode gas streams is defined as:

$$r_d = \frac{\dot{n}_{anode,H_2O,in} - \dot{n}_{anode,H_2O,out}}{I/F} \quad (1.9)$$

Several sources like [Z.Sharaf and F.Orhan, 2014] assume that electro-osmotic drag can be balanced completely by back diffusion. [Berning, 2011] describes the back diffusion as a normal diffusion process and limits the statement of [Z.Sharaf and F.Orhan, 2014] by relating electro-osmotic drag, diffusion and the water content of the membrane. He concludes, that if the water uptake layers are infinite thin, drag and diffusion balance them self. Still the water uptake layer play an important role, as they are not infinite thin.

Another criterion to understand the conditions in a fuel cell, is the dew point of water at the cathode and anode side. As both streams can be humidified gases, dew point diagrams can be set up. These relate the dew point temperature at the anode and cathode outlets with the net drag and are dependent on the net drag coefficient from Equation 1.9, the stoichiometric ratio and the actual pressure [Berning, 2012]. Using these charts, flooding or drying of anode and cathode side can be prevented.

However, the water balance of fuel cells needs to be determined correctly. Therefore numerical methods are combined with tests in laboratories. One of the testing methods is the so called "Hot Wire Anemometry" and is presented next.

1.2 Hot wire anemometry

The idea to use Hot Wire Anemometry in order to detect the fuel cell water balance was first suggested by [Berning and Shakshir, 2015]. A heated wire of constant temperature is placed in the stream. Due to the difference in temperature between the wire (T_w) and the gas at inlet (T_{g1}) heat transfer occurs from the wire to the fluid. From the heat transfer, the gas composition can be estimated. As it is known how much water is fed to the anode and the cathode, the water balance of the cell can be estimated from the composition of the outlet streams.

The heat transfer rate from the wire can be described with Newton's law of cooling:

$$\dot{Q} = A_w \cdot h \cdot (T_w - T_{g1}) \quad (1.10)$$

where:	\dot{Q}	Heat transfer rate	[W]
	A_w	Lateral area of the wire	[m ²]
	T_w	Temperature of the wire surface	[K]
	T_{g1}	Temperature of the gas	[K]
	h	Convective heat transfer coefficient	[Wm ⁻² K ⁻¹]

Equation 1.10 describes the heat transfer due to a difference in temperature from a solid to a fluid. As the heat in the wire is produced by using electricity, it is possible to relate

the power input to the wire and the resistance of the wire with Equation 1.10. However based on King's equation the voltage signal of the wire is only depended on constants, the temperature difference from Equation 1.10 and the Nusselt number [Lomas, 1986]:

$$E = \sqrt{R_w \cdot \pi \cdot L_w \cdot k \cdot (T_w - T_{g1}) \cdot Nu} \quad (1.11)$$

where:	R_w	Resistance of the wire	$[\Omega]$
	L_w	Length of the wire	$[\text{m}]$
	k	Thermal conductivity	$[\text{W m}^{-1} \text{K}^{-1}]$

The Nusselt number is a common dimensionless number, which relates the convective heat transfer to the transport of heat due to conduction [VDI, 2010]. It is defined as:

$$Nu = \frac{h \cdot L_{charc}}{k} \quad \text{and} \quad Nu_{cylinder} = \frac{1}{2\pi} \int_0^{2\pi} Nu_{\phi} d\phi \quad (1.12)$$

where:	h	Convection coefficient	$[\text{W m}^{-2} \text{K}^{-1}]$
	L_{charc}	Characteristic length	$[\text{m}]$
	k	Thermal conductivity	$[\text{W m}^{-1} \text{K}^{-1}]$

The characteristic length in this study is the diameter of the wire D_w . Considering local Nusselt numbers Nu_{ϕ} at a cylinder at angle ϕ , the overall Nusselt number of this cylinder can be calculated with the right part of Equation 1.12 [Haeri and Shrimpton, 2013].

The Nusslet number can be derived out of the two following equations:

$$\dot{q} = \frac{\dot{Q}}{A_w} = h \cdot (T_w - T_{g1}) \quad \text{and} \quad \dot{q} = -k \cdot \left. \frac{\partial T}{\partial x} \right|_{x=0} \quad (1.13)$$

The first part of Equation 1.13 is the specific form of Newton's law of cooling per unit area from Equation 1.10. Furthermore the heat transfer in the boundary layer is assumed to be governed by conduction, which is described by the second part of Equation 1.13. Setting these two Equations equal and reformulating them in terms of the Nusselt number yields the following [VDI, 2010]:

$$Nu = \frac{h \cdot L_{charac}}{k} = \frac{L_{charac} \cdot \left. \frac{\partial T}{\partial x} \right|_{x=0}}{(T_{g1} - T_w)} \quad (1.14)$$

The result in Equation 1.14 contains the characteristic length L_{charac} and shows that is it possible to calculate the Nusselt number based on two ways:

1. Using the thermal conductivity k at film temperature and the convective heat transfer coefficient h estimated based on the heat flow rate e.g.
2. Using the temperature gradient at the wall and the temperature difference

The Nusselt number is dependent on the Reynolds number and the Prandtl number, when considering forced convection. If natural convection is the driving force, the Nusselt number can be written in terms of Grashof and Prandtl number [VDI, 2010]:

$$Nu = f_1(Re, Pr) \quad \text{and} \quad Nu = f_2(Gr, Pr) \quad (1.15)$$

The corresponding dimensionless numbers are given below. The Reynolds number relates inertial forces with viscous forces of the fluid, the Prandtl number relates the viscous diffusion rate with the thermal diffusion rate and the Grashof number relates forces caused due to buoyancy with the viscous forces. All material properties of the listed dimensionless numbers are usually calculated at the film temperature. This temperature is defined as $T_{film} = 0.5 \cdot (T_w + T_\infty)$ [VDI, 2010].

$$Re = \frac{u \cdot L_{charac}}{\nu} \quad \text{and} \quad Pr = \frac{\nu \cdot c_p \cdot \rho}{k} \quad \text{and} \quad Gr = \frac{L_{charac}^3 \cdot g \cdot \beta \cdot \Delta T}{\nu^2} \quad (1.16)$$

Equation 1.15 shows that the heat transfer depends on two different phenomena: forced convection and natural convection. As long as only one phenomenon is the driving force, formulae like the Churchill and Bernstein equation, the Karner approach or the equation after Gnielinski can be used to gain results for the Nusselt number [VDI, 2010]. Berning and Shakshir [2015] showed that none of these equations should be used to identify the Nusselt number of humidified hydrogen streams. Instead the power-law equation by Hilpert [1933] gives good approximation to test results:

$$Nu = C \cdot Re^m \cdot Pr^n \quad (1.17)$$

The coefficients m and C have to be estimated experimentally, while n is usually chosen to be $1/3$. For Reynolds numbers of air streams between 0.4 and 4, m and n are identical and C is 0.989 Hilpert [1933].

The power law by Hilpert [1933] might be accurate, but most of the experiments were conducted at high Reynolds numbers. This causes the demand to validate the power-law for the purpose of this study.

Therefore Equation 1.10 and Equation 1.12 have to be used to calculate the Nusselt number. But there are still two unknowns:

- \dot{Q} - the rate of heat flow from the wire into the fluid
- h - the convective heat transfer coefficient

At first \dot{Q} needs to be determined. Therefore different ways can be used:

- As the power input to the wire is known, it can be used as a heat input
- The first law of thermodynamics relates inlet (T_{g1}) and outlet (T_{g2}) temperatures which can be used to calculate the rate of heat flow

$$\dot{Q} = \dot{m} \cdot \Delta h = \dot{m} \cdot (T_{g2} - T_{g1}) \cdot c_p \quad \text{with} \quad \Delta h = (T_{g2} - T_{g1}) \cdot c_p \quad (1.18)$$

Equation 1.18 considers a steady-state situation of a mass flow that is heated by a heat source. The difference in specific enthalpy Δh can be expressed in ways of temperature, by using the isobaric heat capacity of the fluid and the temperature of the fluid at the

entry and at the outlet of the duct.

Now that the rate of heat flow into the fluid is known, the overall convective heat transfer coefficient can be calculated with Equation 1.10 and allows to set up an expression for the overall Nusselt number:

$$Nu = \frac{\dot{m} \cdot c_p \cdot (T_{g2} - T_{g1}) \cdot L_w}{A_s \cdot (T_w - T_{g1}) \cdot k} \quad (1.19)$$

The Nusselt number described in Equation 1.19 can be interpreted as an overall Nusselt number and is dependent on the mass flow and at least one c_p value.

Assuming the heat input into the wire is known, e.g based on the electrical input or as a result of a simulation, Equation 1.10 can be used directly to calculate h . Furthermore reformulating and inserting this in 1.12 leads to the following formulation:

$$Nu = \frac{\dot{Q}}{\pi \cdot L_w \cdot k \cdot (T_w - T_{g1})} \quad (1.20)$$

It may be noticed, that Equation 1.20 is independent of the wire diameter. Only the length of the wire, L_w plays a role. Furthermore, compared to Equation 1.19 only one material property is needed, what may cause less deviations.

Computational model 2

This chapter will give an overview about the way of modeling the hot wire. That includes the governing equations and the calculation of mixture properties.

2.1 Governing Equations - General approach

To solve a flow related with heat transfer the conservation of mass-, momentum- and energy has to be fulfilled. The fluid is thereby considered to be a continuum, where the smallest fluid element is still very large compared to the distance between the molecules. This can be validated with the Knudsen number [Schlichting and Gersten, 2014].

The conservation of mass states that the incoming and outgoing mass has to be equal to the change in mass due to the changes of density over time [Schlichting and Gersten, 2014].

The density is dependent on the gas composition, defined by the universal gas constant R ($8.314 \text{ J mol}^{-1} \text{ K}^{-1}$), the molar mass of the composition M , the pressure and the temperature. In cases of very low Mach numbers the fluid can be considered as incompressible. In these cases the density is only a function of temperature and composition.

Next the momentum needs to be conserved. Therefore the Navier-Stokes equation is used:

$$\rho \left(\frac{\partial \vec{u}}{\partial t} + \vec{u} \cdot \nabla \vec{u} \right) = -\nabla p + \text{div}(\tau) + \rho \cdot \vec{g} \quad (2.1)$$

Equation 2.1 conserves the momentum of any flow [Schlichting and Gersten, 2014]. The first part of the left hand side is the change of momentum over time, which equals zero in steady-state simulations and the gradient of momentum due to velocity. On the right hand side forces due to the gradient of pressure, the divergence of the viscous stress tensor $\text{div}(\tau)$ and the body force are given [Horacio J. et al., 2013].

The viscous stress tensor is dependent on the assumptions that are made. In case of an Eulerian fluid, it is zero as viscous forces are neglected.

The fluid in this study is a Newtonian fluid, which includes viscous forces. Therefore τ is the following:

$$\tau = \mu \left(\nabla^2 \vec{u} - \frac{2}{3} \cdot \text{div}(\vec{u}) \right) \quad (2.2)$$

Besides the conservation of mass and momentum the energy needs to be conserved as well.

$$\rho \frac{De}{Dt} = \text{div}(k\nabla T) + \tau_{ij} \frac{\partial u_i}{\partial x_j} \quad (2.3)$$

Equation 2.3 is the energy equation for fluid motion [White, 2006]. It contains the change of internal energy, which has to be equal to the heat flow into the control volume, represented by $div(k\nabla T)$ and the energy dissipated due to fluid motion $\tau_{ij} \frac{\partial u_i}{\partial x_j}$.

2.2 Governing Equations - Boussinesq approximation

A simplified approach is the so called Boussinesq approximation, which is valid for flow with small variations in density and temperature. Although the temperature difference might be relatively high, this approximation can be used due to the relatively small differences in density: The heat input from the hot wire is rather low and it can therefore be assumed that the density change is small and does not have an effect on the flow field except for the flow due to buoyancy [Comsol-Multiphysics-Cyclopedia]. Due to the constant material properties, this approximation is not used in this study, but presented here to give a good overview about the modeling techniques that are possible.

At first the mass conservation is achieved using the continuity equation. Due to the assumption of negligible density variations in the main flow field, the incompressible assumption leads to reduced continuity equation:

$$\nabla u = 0 \quad (2.4)$$

Secondly the Navier Stokes equations are solved based on the assumption of constant density ρ_0 except for the buoyant term:

$$\rho_0 \cdot \left(\frac{\partial u}{\partial t} + u \nabla u \right) = -\nabla p + \nabla \tau + \rho \cdot g \quad (2.5)$$

where:

$\rho \cdot g = (\rho_0 + \Delta\rho)g$	Buoyancy term
$\Delta\rho = \rho - \rho_0$	Density change
$\beta = \frac{1}{T_0}$	Thermal expansion coefficient
ρ_0	Density unaffected by heat

The Navier Stokes equation in Equation 2.5 already contain the reference density ρ_0 , which is assumed to be constant and the buoyancy term on the right side, which includes the density change due to thermal expansion. The thermal expansion for ideal gases is the reciprocal value of the initial temperature.

$$\Delta\rho \cdot g = (\rho - \rho_0) \cdot g = -\rho_0 \cdot \beta (T - T_0) \cdot g \quad (2.6)$$

The density change can be rewritten in terms of a temperature change, shown in Equation 2.6. The buoyant forces per unit volume are thereby only dependent on the local temperature T and the unaffected temperature T_0 [Comsol-Multiphysics-Cyclopedia].

Inserting Equation 2.6 in the Navier Stokes equation yields the Boussinesq approximation:

$$\rho_0 \left(\frac{\partial u}{\partial t} + u \cdot \nabla u \right) = -\nabla p + \nabla \tau + \rho_0 \cdot g - \frac{\rho_0 (T - T_0) g}{T_0} \quad (2.7)$$

This set of equations can be solved by the buoyantBoussinesqSimpleFoam solver [OpenFOAM, a].

2.3 Critical Reynolds number

Until now the flow is considered to be laminar. With an increase in velocity, turbulent effects like the energy dissipation in eddies become more important. Different ways of solving turbulent flow can be used. Two very common techniques are, the Reynolds Averaged Navier Stokes (RANS) equations and Large Eddy Simulations (LES). As the velocities in this study are very low there should be no need for RANS modeling nor LES simulation. Therefore the critical Reynolds numbers for flow around a cylinder and for flow in a pipe are needed. This number describes the point of transition from laminar to turbulent flow. Calculating these ensures that the flow is definitely laminar and excludes thereby modeling mistakes.

Kumar and Mittal [2004] investigated the critical Reynolds number for flow around a cylinder and compared it with results of other researchers. In all these cases the critical Reynolds number was larger than 45.

Based on the kinematic viscosity of dry hydrogen at 85°C, the definition of the Reynolds number in Equation 1.16 and the diameter of the wire ($5\mu\text{m}$), it is possible to calculate an approximation for the needed velocity to reach $\text{Re}=45$:

$$u_{w,crit} = \frac{Re_{critical} \cdot \nu}{D_w} = \frac{45 \cdot 1.655 \cdot 10^{-4} \text{m}^2/\text{s}}{5 \cdot 10^{-6} \text{m}} = 1490 \frac{\text{m}}{\text{s}} \quad (2.8)$$

Equation 2.8 shows that approximately 1490 m s^{-1} are needed to reach the critical Reynolds number for flow past a cylinder.

Furthermore the critical Reynolds number for flow in a pipe is defined to be 2300 [Schlichting and Gersten, 2014]. One may notice that Schlichting and Gersten [2014] compared the critical Reynolds numbers of different researchers and stated, that dependent on the incoming flow, critical Reynolds numbers of 40000 or 2000 can be achieved. As 2300 is a commonly used value, it is the limit for laminar flow in a pipe in this study.

Similar to Equation 2.8, the critical velocity for a pipe can be estimated based on the pipe diameter (6 mm) and the corresponding critical Reynolds number. Inserting the values gives a critical velocity of $u_{p,crit}$ of 63 m s^{-1} .

Finally these two calculations have to be interpret correctly: The critical velocities are extreme values and should not be reached. Furthermore the influence of different gas compositions nor the temperature input from the wire on the viscosity is not considered here. Instead the critical values of velocity show, that due to much lower velocities the laminar flow assumption is a valid. Still the actual Reynolds number of each case has to be checked respectively.

2.4 Mixture properties

The mixtures in this study are binary mixtures of dry hydrogen and water vapor, which are assumed to be a perfectly mixed gas. From the tests done by Berning and Shakshir [2015] the mass flow rates of the two species at temperature (T) and pressure (p) are known. As the pressure is assumed to be constant, the properties are only dependent

temperature.

To validate these results, the thermo physical properties of the fluid need to be calculated depending on its composition. As the flow rates and the molecular weights of the species are known, the molar and mass fractions can be calculated. These have to equal one, when summing them up.

The heat capacity and the density of a mixture of ideal gases can be calculated based on the mass fractions y_i and the properties of each species:

$$c_{p,mix} = \sum_1^i c_{p,i} \cdot y_i \quad \text{and} \quad \rho_{mix} = \sum_1^i \rho_i \cdot y_i \quad (2.9)$$

where: $c_{p,i}$ | Specific heat capacity of species i [J kg⁻¹ K⁻¹]
 y_i | Mass fraction of species i [-]

The dynamic viscosity and the thermal conductivity of binary mixtures can be calculated using the following formula:

$$\phi_{mix} = \frac{x_1 \phi_1}{x_1 + x_2 A_{12}} + \frac{x_2 \phi_2}{x_2 + x_1 A_{21}} \quad (2.10)$$

In Equation 2.10 ϕ represents the property, x_i the molar fraction of a species i and A_{ij} represents a function dependent on the property that is calculated [Wilke, 1950].

When the dynamic viscosity is calculated, these coefficients are defined as:

$$A_{12} = \frac{\left[1 + \left(\frac{\mu_1}{\mu_2} \right)^{0.5} \cdot \left(\frac{M_2}{M_1} \right)^{0.25} \right]^2}{\left[8 \cdot \left(1 + \frac{M_1}{M_2} \right) \right]^{0.5}} \quad (2.11)$$

and

$$A_{21} = \left(\frac{\mu_2}{\mu_1} \right) \cdot \left(\frac{M_2}{M_1} \right) \cdot A_{12} \quad (2.12)$$

When the thermal conductivity needs to be estimated A_{12} and A_{21} are defined as:

$$A_{12} = 1.144 \frac{\alpha_1}{D_{12}} \quad \text{and} \quad A_{21} = \frac{\alpha_2 \cdot D_{12}}{\alpha_1 \cdot D_{21}} A_{12} \quad (2.13)$$

Equation 2.13 uses the thermal diffusivities of the pure species (α) and the binary diffusion coefficients D_{12} . In binary mixtures the binary diffusion coefficient D_{12} equals D_{21} [Wilke, 1950].

2.4.1 Temperature dependent fluid properties

The way of calculating mixture properties, which was shown in Chapter 2.4, gives only results for one temperature, respectively. As the temperature in the domain is locally different, fluid properties need to be dependent on the temperature. Therefore polynomial functions are set up, based on fluid properties at different temperatures. These properties

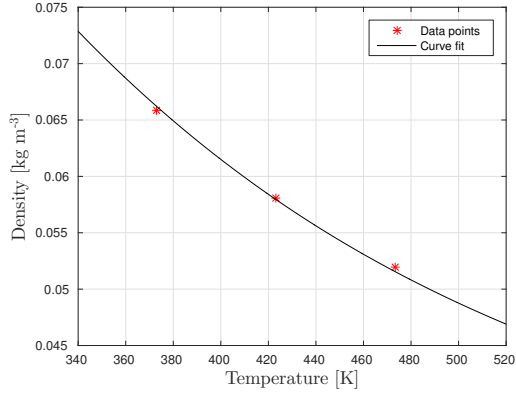


Figure 2.1. Curve fit for the density of dry hydrogen.

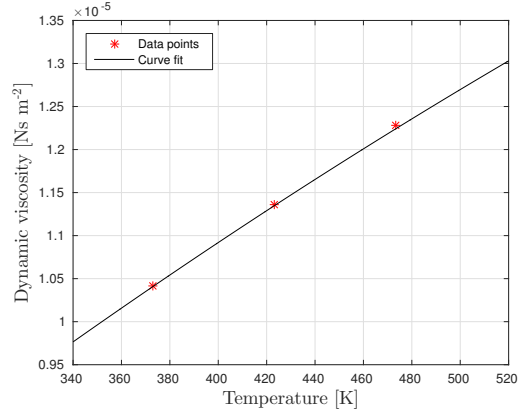


Figure 2.2. Curve fit for the dynamic viscosity of dry hydrogen.

were chosen in a range that is not expected to exceed during the simulations. Exemplary these curves are shown here for dry hydrogen in the expected range.

Figure 2.1, 2.2 and 2.3 show the curve fits of the density, the dynamic viscosity and the thermal conductivity of dry hydrogen. The curves are at least second order polynomials and fit the data points with an accuracy of R^2 of more than 0.99. This indicates that the fitted functions describe the data points very good. Besides the R^2 value it can be seen that the curves lay relatively smooth on the data points. Small deviations have to be interpreted correctly: Although only three data points are shown, the curves are based on seven different points and each curve fits these satisfactory.

The curve fit of the specific heat capacity is shown in Figure 2.4 and is a polynomial

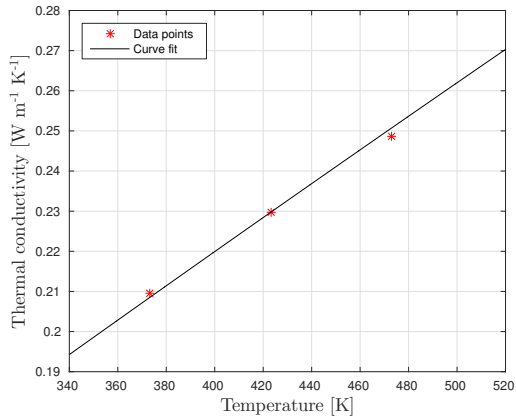


Figure 2.3. Curve fit for the thermal conductivity of dry hydrogen.

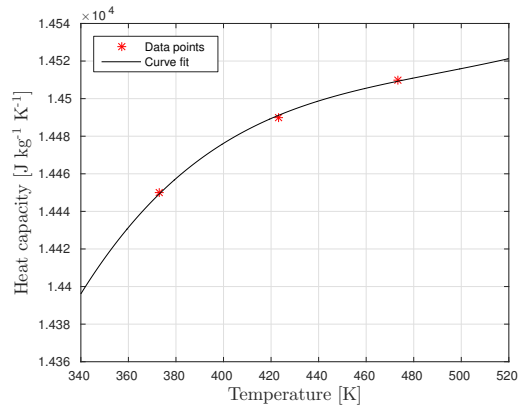


Figure 2.4. Curve fit for the heat capacity of dry hydrogen.

function of 4th order. The R^2 value is again above 0.99.

Overall, the presented curves are accurate enough to use them as an input for the simulations.

In cases with humidified hydrogen, the polynomial functions show similar shapes. The order of the functions was chosen individually dependent on the local steepness.

All data and functions can be found in Appendix A.2.

Analytical considerations

3

From Chapter 1.2 it is known that the Nusselt number can be calculated by using the power law, which is based on the Prandtl and the Reynolds number at the wire.

Due to the fact of having internal and laminar flow, it is expected to have a developed velocity only dependent on the radius. As the wire is placed in the middle, it experiences the maximal velocity in the two dimensional case. If the Reynolds number at the wire is calculated based on the average velocity (volumetric flow over area), it is actually not the correct velocity due to the mentioned velocity profile.

The CFD gives the possibility to gain the profile, but it is rather time consuming and it is desired to have a correction that is useful to correct experimental data.

Therefore a formulation can be derived from the Navier Stokes equations which is known as Hagen-Poiseuille Flow [Schlichting and Gersten, 2014]. The following picture depicts the situation of laminar flow.

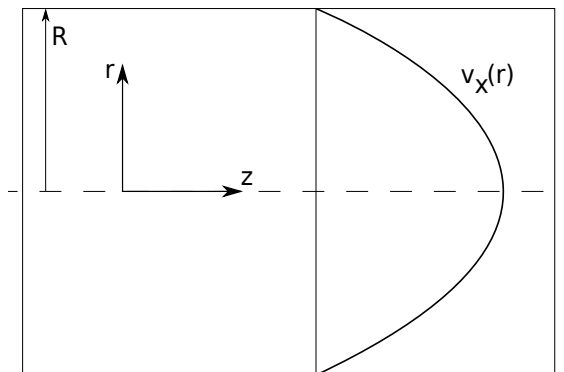


Figure 3.1. Hagen-Poiseuille Flow in a pipe.

The shown profile of the velocity ($v_x(z)$) is a parabolic function and thereby only dependent on the radial component r .

3.1 Hagen-Poiseuille flow in a pipe

At first the correlation for internal pipe flow is derived. Therefore the Navier-Stokes equations in cylindrical coordinates in flow direction is needed [Schlichting and Gersten, 2014]:

$$\rho \left(\frac{\partial v_x}{\partial t} + u_r \frac{\partial v_x}{\partial r} + \frac{v_\phi}{r} \frac{\partial v_x}{\partial \phi} + v_x \frac{\partial v_x}{\partial x} \right) = -\frac{\partial p}{\partial x} + \mu \left[\frac{1}{r} \frac{\partial}{\partial r} \left(r \frac{\partial v_x}{\partial r} \right) + \frac{1}{r^2} \frac{\partial^2 v_x}{\partial \phi^2} + \frac{\partial^2 v_x}{\partial x^2} \right] \quad (3.1)$$

Equation 3.1 already neglects forces due to gravity. The following assumptions are made to solve the equation analytically:

- The flow is steady-state $\rightarrow \frac{\partial(\dots)}{\partial t} = 0$
- No rotational nor swirled flow is considered $\rightarrow v_r = v_\phi = 0$
- The flow is considered to be axis symmetric $\rightarrow \frac{\partial(\dots)}{\partial \phi} = 0$
- and fully developed $\rightarrow \frac{\partial v_x}{\partial x} = 0$

With these assumptions Equation 3.1 can be simplified to the following statement:

$$\frac{\partial p}{\partial x} \frac{1}{\mu} r = \frac{\partial}{\partial r} \left(r \frac{\partial v_x}{\partial r} \right) \quad (3.2)$$

Integrating this equation twice leads to the following statement:

$$v_x = \frac{1}{4\mu} \frac{\partial p}{\partial x} r^2 + A \ln(r) + B \quad (3.3)$$

A and B are constants from the integration and need to be estimated. Therefore the boundary conditions are needed.

- The highest velocity is in the pipe center at $r=0 \rightarrow v_z = v_{\max}$
- The velocity is zero at walls due to the no-slip condition at $r=R \rightarrow v_x = 0$

As A needs to be zero due to the logarithmic function, B equals the following:

$$A = 0 \quad \text{and} \quad B = -\frac{1}{4\mu} \frac{\partial p}{\partial x} R^2 \quad (3.4)$$

Inserting these into Equation 3.3 gives the Poiseuille equation.

$$v_x = \frac{1}{4\mu} \frac{\partial p}{\partial x} (r^2 - R^2) \quad (3.5)$$

Choosing the $r = 0$, Equation 3.6 shows, that the velocity in the center of the pipe is highest:

$$v_{x,max} = -\frac{R^2}{4\mu} \frac{\partial p}{\partial x} \quad (3.6)$$

Furthermore, the velocity reaches zero, if r becomes R . The boundary conditions are thereby fulfilled.

Still the given expression is not directly useful as a pressure gradient is included. The aim is to refer the maximum velocity to the average velocity as this is usually known. First the average velocity is calculated:

$$v_{x,av} = \frac{\dot{V}}{\pi R^2} = \frac{\int_0^R 2\pi r v_x(r)}{\pi R^2} = -\frac{R^2}{8\mu} \frac{\partial p}{\partial x} \quad (3.7)$$

Finally, relating the average and the maximum velocity from Equation 3.6 and 3.7 a simple correlation can be set up:

$$v_{x,max} = 2 \cdot v_{x,av} \quad (3.8)$$

This correlation is valid as long the critical Reynolds number (based on average velocity and pipe diameter) is below 2300 and the flow thereby considered to be laminar [Schlichting and Gersten, 2014]. As the average velocity is usually known, when running tests in the lab, this formulation can be used directly to correct the velocities at the wire.

3.2 Hagen-Poiseuille flow between two not moving parallel plates

The just shown derivation is only valid for internal pipe flow. Considering a two dimensional model, where the hot wire is placed in the center, the flow has to be considered as flow between two parallel plates. The distance to the plates equals in this case the pipe radius. As long as the flow is laminar, a derivation similar to the one shown in Chapter 3.1 can be done.

As the derivation and the assumptions in this case are similar, the derivation is kept short. Together with the no-slip condition and the following assumptions the Navier-Stokes equation can be simplified. Integrating twice and inserting the boundary conditions gives thereby the velocity profile in x-direction:

$$v_x = -\frac{1}{2\mu} \frac{\partial p}{\partial x} (H^2 - y^2) \quad (3.9)$$

y represents in this equation the coordinate normal to the flow and H is half of the channel height. The maximal velocity is obtained again by inserting $y = 0$ and the average by integrating:

$$v_{x,av} = \frac{\int_{-H}^H v_x(y) dy}{2Y} = -\frac{1}{3\mu} \frac{\partial p}{\partial x} H^2 \quad (3.10)$$

Thereby the average and the maximal velocity (at $y = 0$) can be related:

$$v_{x,max} = 1,5 \cdot v_{x,av} \quad (3.11)$$

The two dimensional CFD models should hold this correlation. Otherwise it would be questionable if the set up of these models is correct.

Model description 4

The experiments in the laboratory were previously done with the following setup, shown in Figure 4.1. The gas composition is delivered from the left "H₂-flow in" until the stream flows past the "Hot wire sensor". The outgoing flow is leaving through a pipe after a 90° bend, shown with "H₂ flow out". All relevant test equipment is isolated and heated to keep the gas temperature as constant as possible until the fluid reaches the wire.

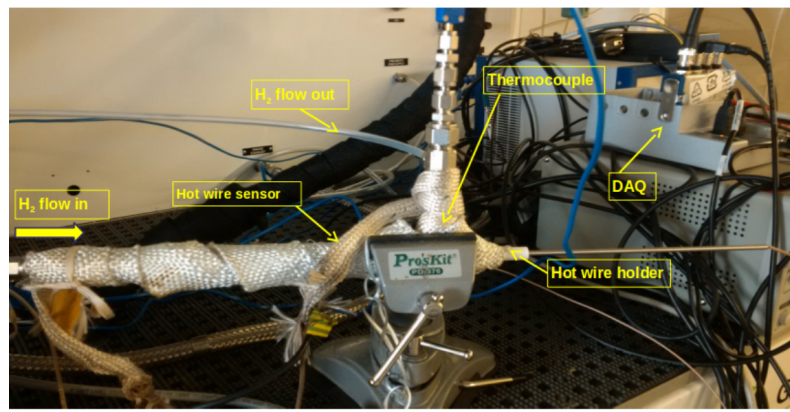


Figure 4.1. Experimental setup - Overall.

The hot wire is kept in position with the "Hot wire holder", which is shown in detail in the next figure and placed in the pipe already. The wire is too small to see it here.

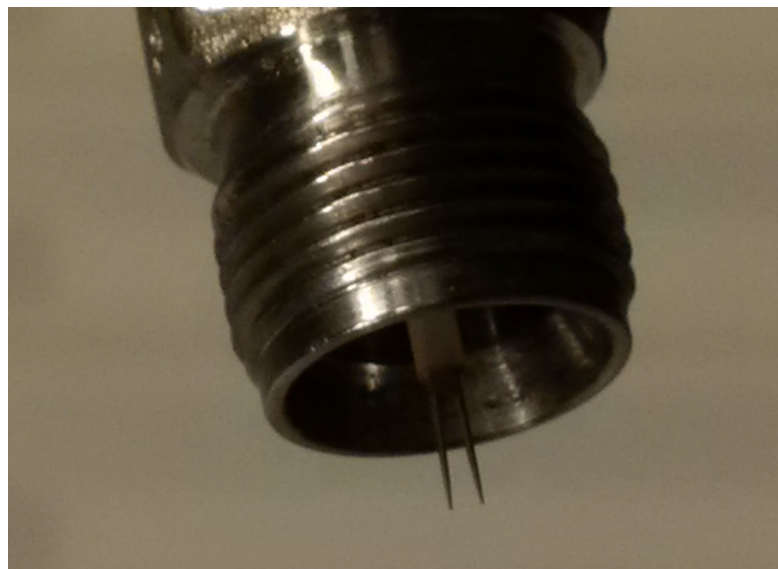


Figure 4.2. Experimental setup - Hot wire with leads.

This experimental setup is simplified to a model, shown in Figure 4.3. The model which is used to represent this setup is shown and described in the following Chapter.

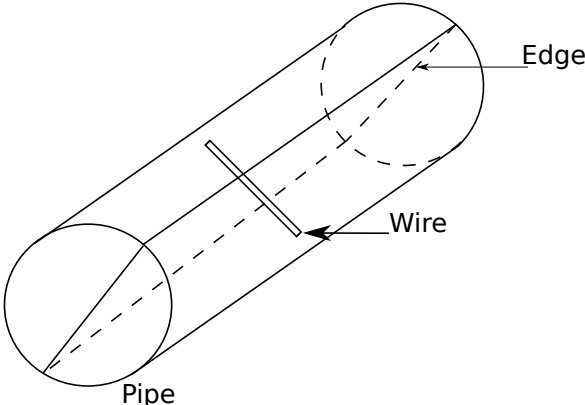


Figure 4.3. CFD model setup.

The setup shown in Figure 4.3 includes only the hot wire without the holding mechanism. Furthermore it is assumed that the pipe is straight.

2D model 5

5.1 Geometric description of the two dimensional model

In order to have a model that is fast to run and easy to adjust, a two dimensional model is build up. This model consists of the hot wire in the center and the dimensions of the pipe around the wire. In Figure 4.3 an edge is shown which is placed in the middle of the pipe. The two dimensional model is build along this edge which is shown in Figure 5.1.

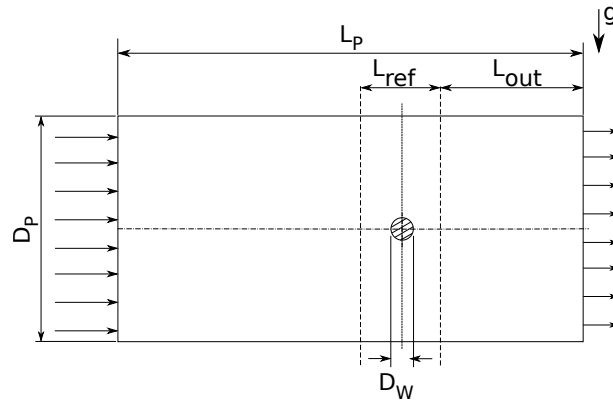


Figure 5.1. 2D model - Dimensions.

The domain shown in Figure 5.1 has an inlet on the left side and the outlet on the right side. To achieve a developed velocity profile and to prevent influences from the wire to the inlet, a pipe segment is placed in front of the wire that is long enough to allow the development.

Abbreviation	Value	Unit
D_p	$6 \cdot 10^{-3}$	m
D_w	$5 \cdot 10^{-6}$	m
L_p	$100 \cdot 10^{-3}$	m
L_{ref}	$10 \cdot 10^{-3}$	m
L_{out}	$30 \cdot 10^{-3}$	m

Table 5.1. 2D model - Dimensions.

Table 5.1 lists the data of the model corresponding to Figure 5.1. D_p and D_w are the diameter of the pipe and the wire, respectively. The lengths L_p , L_{ref} and L_{out} represent the length of the whole pipe segment, the length of the coarse refinement region and the length of the outlet block, respectively.

As the flow is laminar in this study, this length which refers to the entrance region, can be estimated based on an empirical formula [Subramanian]:

$$L_{entrance} \approx D_P \cdot 0.05 \cdot Re_P \quad (5.1)$$

After $L_{entrance}$ the velocity profile is fully developed. This means for the model, that the wire has to be placed behind the entrance region.

5.2 Meshing of the model

The domain is based on a two dimensional mesh and therefore only one layer of cells is needed. These cells are arranged in different sized blocks. A blocking plan can be found in Appendix B. The following mesh quality criteria were used to mesh the geometry:

criteria	Value
Aspect ratio	< 50
Non-orthogonality	< 65
Determinant	> 0.001

Table 5.2. Mesh quality criteria.

As the pipe diameter is 1200 times larger than the wire diameter, the mesh needs local refinements to solve the domain efficient and the flow around the wire properly.

Therefore the mesh can be split into four regions:

- The inlet segment
- The outlet segment
- The pipe segment with the wire in the center
- A refinement region in the pipe segment, which resolves the wire

The inlet segment up to the refinement zone L_{ref} is meshed relatively coarse.

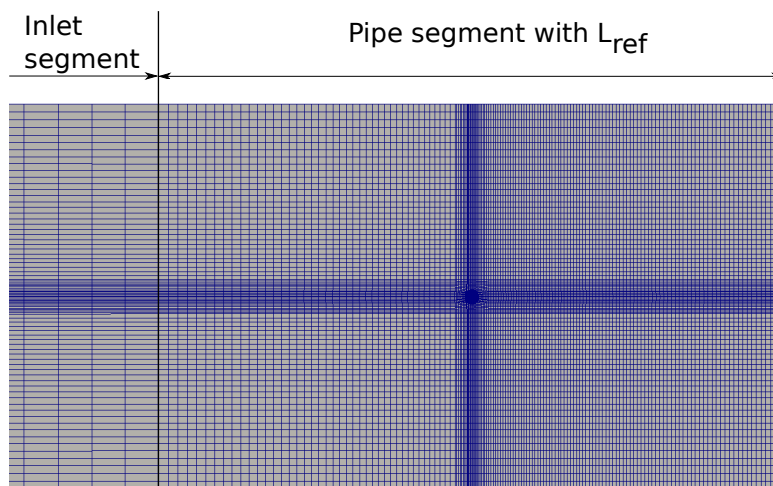


Figure 5.2. 2D model - Meshing.

Figure 5.2 shows the mesh of the inlet segment partly and the pipe segment. It can be seen, that the meshing in the direction of flow is much finer than normal to the direction of flow. Furthermore the pipe segment is meshed finer than the inlet segment. The position of the wire can be seen in the center of the pipe segment as the mesh density is much higher there.

Next the refinement zone around the wire is shown in Figure 5.3.

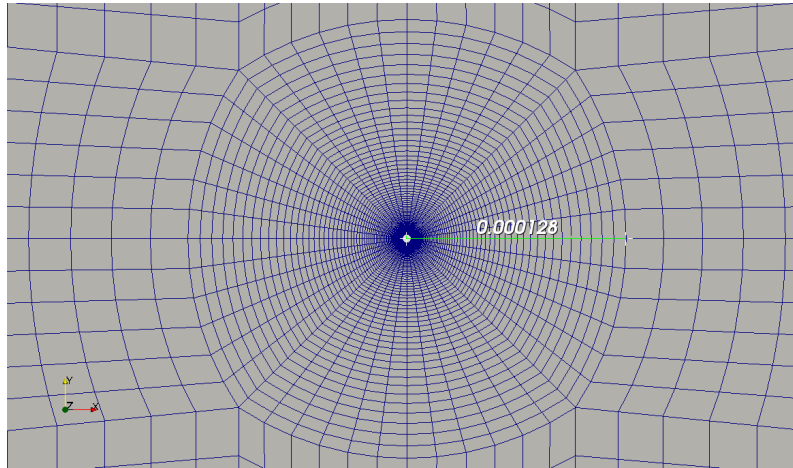


Figure 5.3. 2D model - Meshing around the wire.

This zone has a thickness of 0.128 mm in flow and in normal direction. In total there are 80 cell layers from the wire to end of the refinement zone. Furthermore an expansion ratio of 100 is setup. This achieves thinner cell layers at the wire and thicker cells close to the rest of the mesh. Besides a sufficient resolution close to the wire wall, the mesh quality is improved, as the cell sizes of the refinement zone are of similar size as the cells from the pipe segment around.

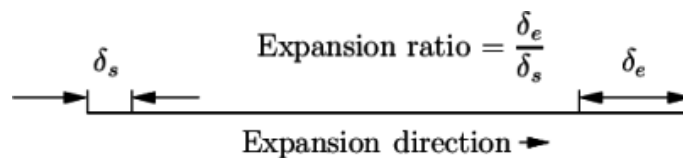


Figure 5.4. 2D model - Expansion ratio [OpenFOAM, b].

The cell thickness close to the wire is thereby 100 times thinner than the thickness of the cells furthest away (refer to Figure 5.4).

Finally grid independence will be shown in Chapter 5.5. As this study includes three models, the process of grid independence is only shown once.

5.3 Boundary definitions

To solve the flow boundary conditions need to be defined. These are listed in Table 5.3.

The condition "fixedValue" defines a fixed value at a boundary. Temperature and velocity have to be defined in this case based on "fixedValue" at the inlet as velocity and

Quantity	Inlet	walls	Wire	Outlet
Temperature [K]	fixedValue	zeroGradient	fixedValue	zeroGradient
Velocity [ms ⁻¹]	fixedValue	fixedValue	fixedValue	zeroGradient
	mapped	no-slip	no-slip	
Static P.(Pa)	calculated	calculated	calculated	calculated
Reduced P. (p_{rgh}) [Pa]	fixedFluxPressure	fixedFluxPressure	fixedFluxPressure	fixedValue

Table 5.3. Boundary definitions.

temperature are known there and assumed to be constant. To achieve realistic velocity profiles close to walls, the no-slip condition is used by forcing the "fixedValue" boundary condition to be 0 ms⁻¹.

The reduced pressure is a quantity, which is defined as $p_{rgh} = p - \rho gh$. OpenFOAM uses therefore the placeholder boundary condition "calculated" for the static pressure "p". "fixedFluxPressure" is a boundary condition, which is in this case equal to the zeroGradient boundary condition. In the OpenFOAM community it is known for better convergence due to a different definition in the source code [CFD-Online, a].

5.4 Interpretation of the two dimensional model

After the presentation of the model, the mesh and the boundary definitions it is needed to highlight the difference between the 2D model and the setup shown in Figure 4.3. Although the flow will still be laminar and result in a typical velocity profile, the values will be not exactly the same as in a fully developed pipe flow. This is due to the simplification of using only two dimensions. Thereby the no-slip condition influences the flow only from two sides and not 360° as in a laminar pipe flow.

This model represents in the end flow between two parallel, infinite long walls. As described in Chapter 1.2 mostly dimensionless numbers are of interest and therefore this approach is still accurate enough as the Reynolds number e.g represents the difference in velocity already.

Another distinction between Figure 4.3 and the model is, that the heat transfer from the wire is only dependent on the free stream velocity in the center of the model. In three dimensional pipe flow, the heat transfer is affected as well by the velocity profile along the axis of the wire.

However, these inaccuracies are acceptable compared to the computational cost caused by three dimensional models. Furthermore the results shown later on, will show if the inaccuracies are actually extreme.

5.5 Grid independence study

The result of a CFD simulation might depend on the mesh resolution. To prove that this is not the case, a grid independence study is done. ERCOFTAC [2000] recommends to double the number of cells twice and compare critical values. If these do not vary significantly but tend to converge towards a value, grid independence can be assumed for that domain.

Besides the mesh resolution, convergence can influence the result as well. Therefore convergence is checked based on residuals and values like temperature and velocity. If the residuals reached a certain value and do not vary anymore the mentioned values are checked for convergence as well. This means if for example the temperature at the outlet does not change anymore with the number of iterations, it can be assumed to be converged. The domain presented in Chapter 5 is refined twice. Only the number of cells in the region around the wire (refer to Figure 5.3) is kept constant, as the mesh resolution is already finest here.

Model	Number of cells
Coarse	14136
Medium	31474
Fine	59892

Table 5.4. Grid independence study - mesh resolution.

The models of different mesh size are based on the same boundary conditions as all other models. These assumptions are listed in Table 5.3. The fluid in this case is dry hydrogen at ambient pressure and the velocity at inlet is defined to be 1.85 m s^{-1} . This results in a Reynolds number at the wire of 0.056 and a Reynolds number of 67 for the pipe. Compared with the values of critical Reynolds numbers in Chapter 2.3, it can be seen that the assumption of laminar flow is valid here.

Based on the given information the values of pressure loss, taken from the inlet and temperature and velocity taken from the outlet are compared. The temperature and velocity are hereby plotted cross sectional 0.2 mm upstream from the outlet.

At first the pressure loss of the three simulations is shown in Figure 5.5. One may notice that the pressure is given in milli-Pascal. It can be seen, that with duplication in cells

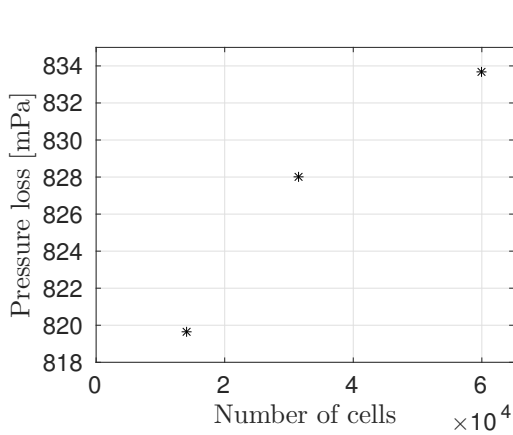


Figure 5.5. Grid independence study - Pressure loss.

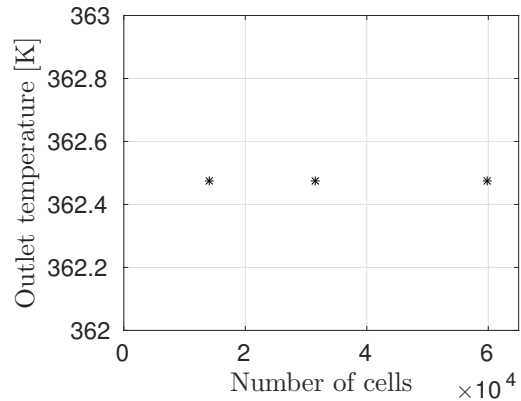


Figure 5.6. Grid independence study - Averaged temperature at outlet.

from the coarse to the medium mesh, the pressure loss increases from approximately 819.6 mPa to 828 mPa. That is an increase of 1.1%.

When doubling the number of cells again, the pressure loss still increases and reaches approximately 833.7 mPa. The percentile change between the medium mesh and the fine

mesh is 0.7%.

Based on the behavior of pressure loss one already can conclude grid independence as the pressure loss seems to converge towards a value and the change is below 1%.

Besides the pressure loss, the averaged temperature at the outlet is plotted in Figure 5.6. It can be seen, that the averaged temperatures are identically, what supports the assumption of grid independence. However, the pressure loss and the averaged temperature are good indicators, but it is safer to consider not averaged values as well.

Therefore the profiles of absolute velocity and temperature close to the outlet are

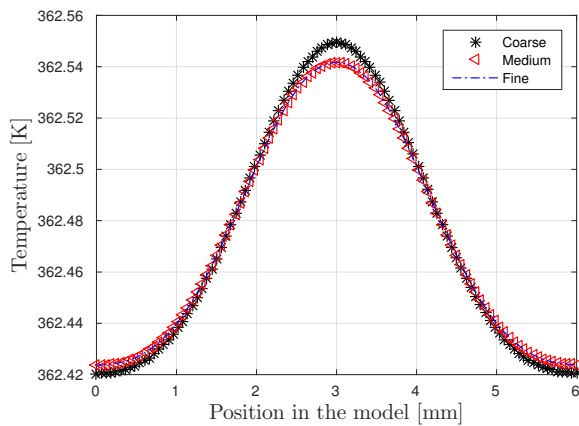


Figure 5.7. Grid independence study - Temperature profile.

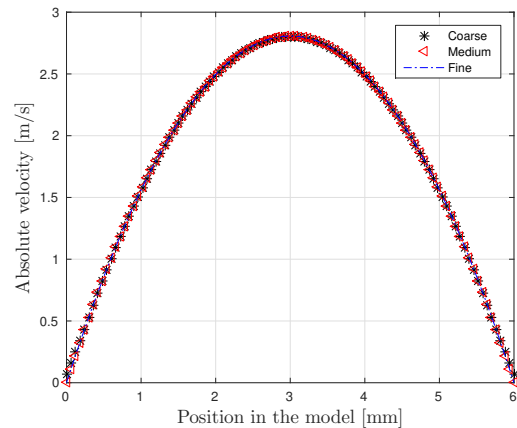


Figure 5.8. Grid independence study - Velocity profile.

compared. From Figure 5.7 it can be seen, that the temperature profiles of all the three meshes are very similar. Only the coarse mesh seems to differ from the other two in the center and close to the walls of the pipe. Between the medium and the fine mesh no difference can be seen.

Considering the velocity profiles in Figure 5.8, it can be seen that the curves are visually identical.

From these graphs it can be concluded that the medium and the fine mesh will give grid independent results as their pressure loss, averaged temperature and temperature and velocity profiles give very similar up to identical results. A model with fewer cells than the medium mesh is not recommended in this case as the temperature profile varies from the finer meshed models.

Furthermore the velocity profiles, shown in Figure 5.8, show as well physical behavior: Due to the no-slip condition at the walls, the velocity must equal zero at the walls. As the velocity at the inlet is defined as 1.85 m s^{-1} the core flow speeds up after the inlet because the flow close to walls has to show a velocity profile. Additionally the velocity profiles correspond to the shape of laminar velocity profiles in pipes [Schlichting and Gersten, 2014]. Based on the results from the Hagen-Poiseuille flow in Chapter 3.1 the maximal velocity should be 1.5 times larger than the average velocity. With the given velocity the maximal velocity based on Hagen-Poiseuille is 2.775 m s^{-1} . From Figure 5.8 it can be seen, that the maximal velocity is approximately 2.8 m s^{-1} .

However, based on the shown figures it can be concluded that grid independence is given for the medium and the fine mesh. The medium mesh is chosen to do the study, as it is accurate enough and more efficient than the fine mesh.

5.6 CFD simulation start cases

This study contains results of different simulations. The humidified cases are based on dry hydrogen cases. This means that the flow rate of hydrogen of one case is kept constant, while the flow rate of water vapor is increased from 0% RH up to 100% RH.

Table 5.5 lists all cases simulated with hydrogen at 0% RH. In the left column the case name is given, which is related to the folder name in the enclosure. Next the inlet velocity is given, followed by the corrected Reynolds (refer to Chapter 3.2) number at the wire.

Case	Inlet velocity Dry H ₂ [m s ⁻²]	Corrected Reynolds number at the wire
06-01	2.00	0.073
06-02	1.4744	0.054
06-03	1.1795	0.043
06-04	0.8846	0.032
06-05	0.58988	0.021
06-06	0.2949	0.011
06-07	0.1474	0.005

Table 5.5. Dry hydrogen - Case overview.

The case numbers correspond to the folder names, which are listed and explained in Appendix C.

It may be noticed, that the listed cases needed between 10^5 and $8 \cdot 10^5$ iterations until convergence was achieved.

5.7 Influence of the hot wire on the surrounding

Besides a comparison of the coefficients for the power law that describes the Nusselt number, this study is carried out to gain knowledge about the influence of the wire to the surrounding.

Following questions shall be answered in this chapter:

- Does heat diffuse upstream?
- Is the approach of using the film temperature correct?
- Does natural convection play a role?

Of course the error that might be done by using the film temperature would be the same in case of the CFD simulations and the results from the laboratory, but it is still of interest if there is a limitation of using this approach.

All listed points are related to similar situations of having low velocities that transport the heat away from the heat source. A dimensionless number that gives an approximation of this is the Peclet number which is the multiplication of the Reynolds and the Prantl

number. It gives an approximate insight if a property is transported due to convection or diffusion.

Figure 5.9 shows the Peclet number as a function of the Reynolds number based on pipe diameter at inlet conditions. It can be seen, that all cases have a Peclet number >1 what indicates that the convective transport has a higher impact than diffusive. Still the lowest number reaches a Peclet number smaller than 5 and it cannot be concluded just from this, if the temperature field diffuses partly upstream.

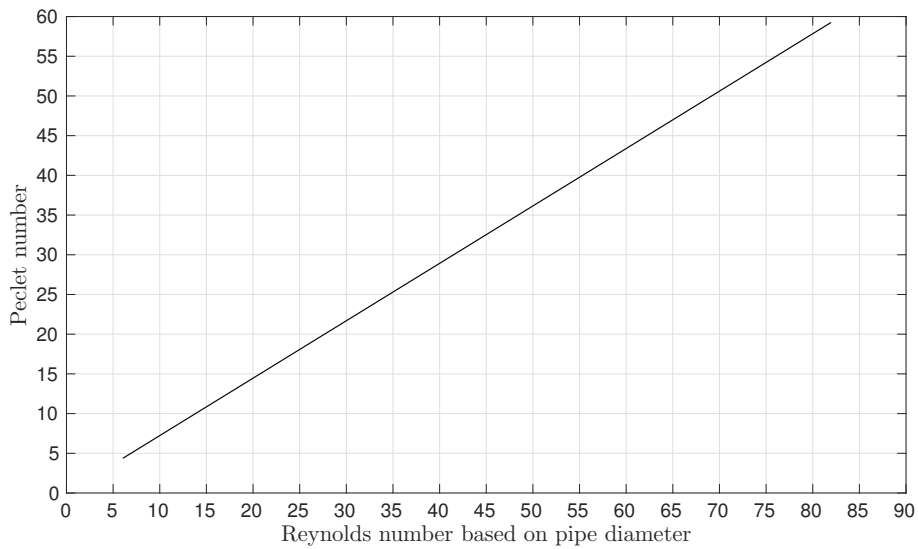


Figure 5.9. Dry hydrogen - Peclet number based on inlet properties at 85°C.

Therefore data is taken from the domains along the center line, shown in Figure 5.10.

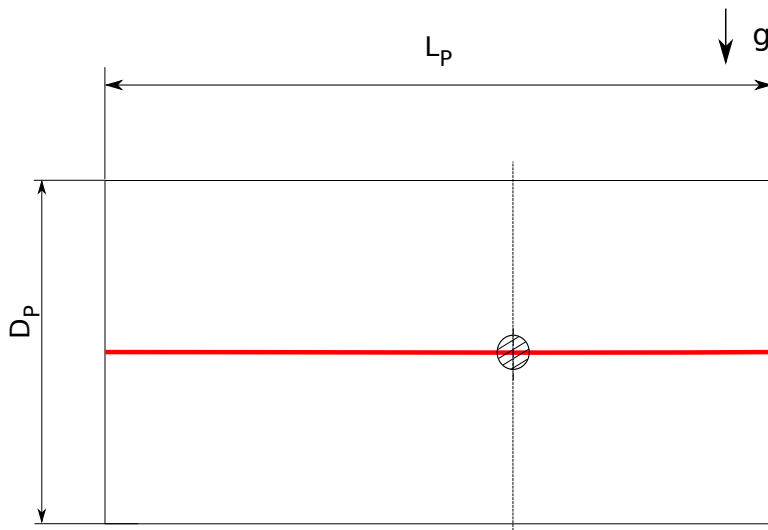


Figure 5.10. Lines for data extract.

At first it is of interest to validate the axial velocities in the center to gain knowledge about the influence of the wire to the region downstream. The following figure shows

these velocities along the center line for all simulated cases of dry hydrogen. It may be noticed that the model length is normalized with the length of the domain. Thereby the inlet is at "0", the outlet at "1" and the wire is placed at "0.7" and marked with a vertical black line.

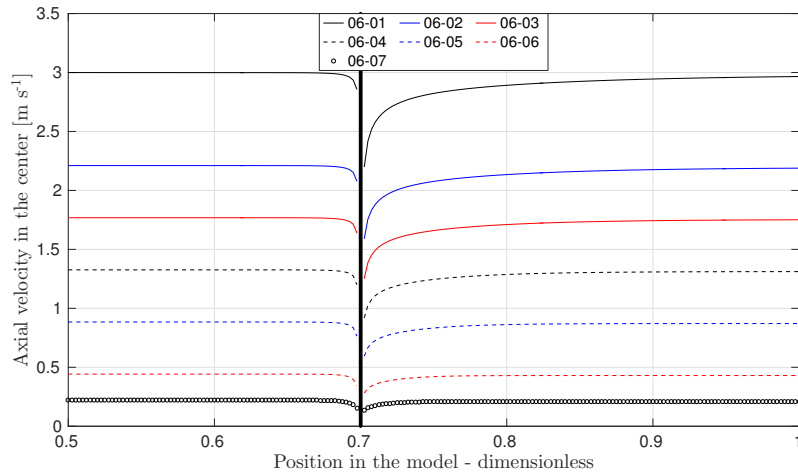


Figure 5.11. Dry hydrogen - Axial velocities in the center.

The legend in Figure 5.11 lists the cases based on their case names corresponding to Table 5.5. From the figure it can be seen, that the velocity relation based on Hagen-Poiseuille is fulfilled precise, as all cases have a 1.5 times larger maximal velocity than the average inlet velocity.

It can be observed that the velocity is slowed down due to the no-slip condition at the wire. Behind the wire, the flow speeds up again and it can be seen, that a higher velocity results in a longer distance behind the wire until the velocity reaches initial conditions again. This is due to the transport of momentum normal to the flow: The transport of momentum normal to the flow occurs relatively faster, if the mainstream velocity is low compared to high velocities.

As the velocities are evaluated and validated, the influence of the velocity to the outlet temperature is of interest as well. The following figure represents the averaged temperature at the outlet of the CFD models. The boundaries listed in Table 5.3 define a constant temperature at the inlet. This was chosen to be 85°C (358.15K) in all simulations.

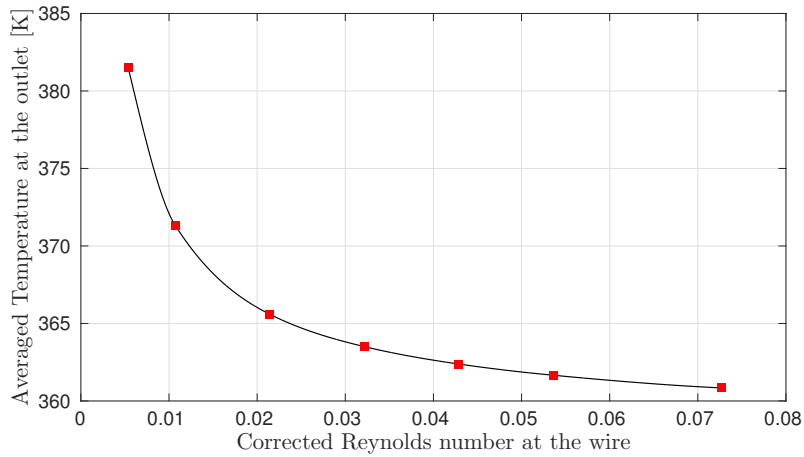


Figure 5.12. Dry hydrogen - Averaged outlet temperature in relation with the Reynolds number.

The velocity is written in terms of the corrected Reynolds number of the wire and from Figure 5.12 it can be seen that the outlet temperature is strongly dependent on this number. The shown curve can be interpreted as an exponential function, as it will never reach the inlet temperature of 358.58 K. Between approximately $Re \approx 0.005$ (Pe at inlet ≈ 4.4) and $Re \approx 0.02$ (Pe at inlet ≈ 17.5) the curve is very steep.

The shown graphs indicate already, that the hot wire has an influence on its surrounding and the flow downstream, but it is still unknown how the temperature develops upstream from the wire. Therefore the temperature along the center line is presented next.

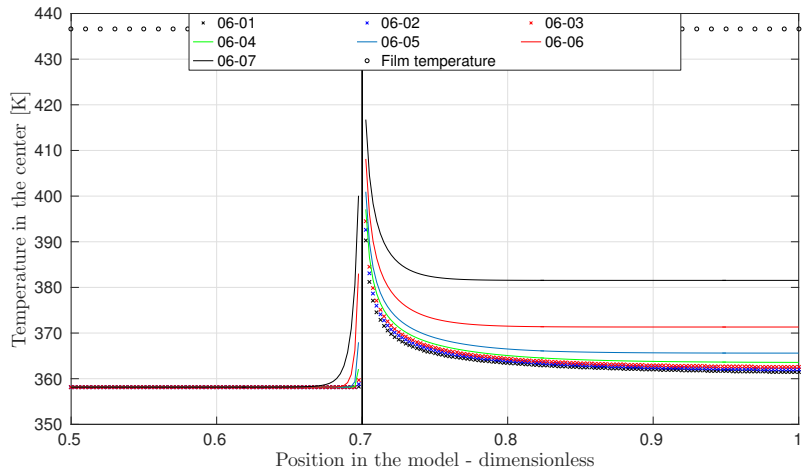


Figure 5.13. Dry hydrogen - Temperature in the center.

From Figure 5.13 a tendency can be concluded: The lower the velocity is, the more upstream will the temperature field develop. Especially in the case with lowest inlet velocity it can be seen, that heat diffuses approximately 0.1 cm upstream. Furthermore compared with Figure 5.12, the same tendency can be seen: The lower the velocity is, the higher is the temperature at the outlet.

The first question of this section was if heat diffuses upstream and the second question if the film temperature is still a good approximation. Based on the shown material, it can be concluded that although heat diffuses upstream the film temperature seems

to be a correct approach. VDI [2010] defines the film temperature as the following: $T_{film} = 0.5 \cdot (T_w + T_\infty)$, where T_∞ is the inlet temperature in the presented cases. Although the definition of the film temperature gives a clear answer about the temperature, there is no definition directly related to the film temperature thickness.

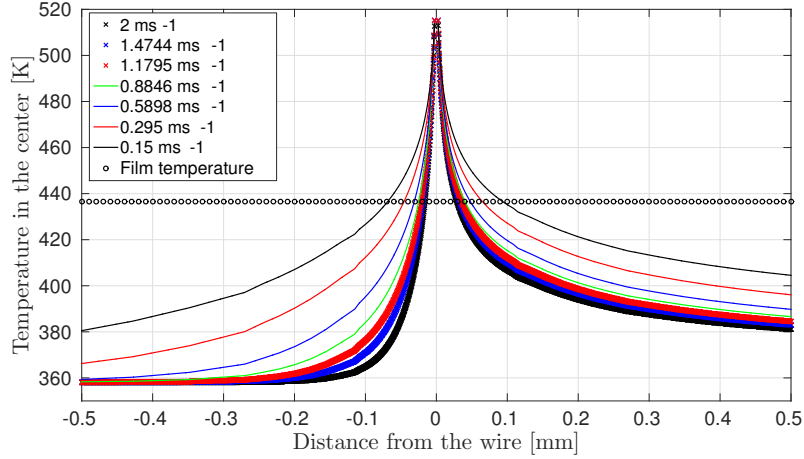


Figure 5.14. Dry hydrogen - Temperature in the center in comparison with the film temperature.

With the given definition the film temperature is 436.65 K in the presented cases. Considering Figure 5.13 it can be seen that although heat diffuses upstream, the film temperature is a good choice, as the temperature profile at the wire is very narrow. As it is hard to see, a new figure shall show a range 0.5 mm up- and downstream the wire. This is shown in Figure 5.14 and it can be seen, that the thickness of the film temperature layer is not symmetric but still very thin. Even in Case 06-07 with the lowest velocity (0.15 m s^{-1} inlet velocity) the distance to the wire at 436.15 K is less than 0.1 mm. The higher the velocity is, the smaller is thereby the thickness of the film temperature.

From the figure it can therefore be concluded, that the film temperature is still valid to calculate material properties at the wire. It has to be kept in mind that with even lower velocities than the presented ones the thickness increases and at some point it may be that the film temperature is not a good choice anymore.

Last, the impact of natural convection has to be estimated. Therefore vector plots are used. These are taken from a plane of $1 \cdot 10^{-5} \text{ m}$ in positive and negative direction respectively. The wire is placed in the center. To allow the reader a good understanding, the described situation is shown in Figure 5.15. From the figure it can be seen how small the plot region is. In case of natural convection, the velocity vectors would be aligned against the direction of gravity. Such a case is shown in Figure 5.16 described by White [2006]. Although the natural convection Figure 5.16 is not represented based on vectors, the effect can be seen: As the gravity acts downwards, the flow direction is upwards. Thereby the flow regime is alike the regimes of creeping flow ($Re \rightarrow 0$) up to the low Reynolds region of vortex pairs in a wake ($3-4 \leq Re \leq 30-40$) [Schlichting and Gersten, 2014]. It may be noticed that the Rayleigh number of the shown case is approximately 10^5 . The number is defined as the product of Prandtl and Grashof number [White, 2006]. In case of the hot wire of

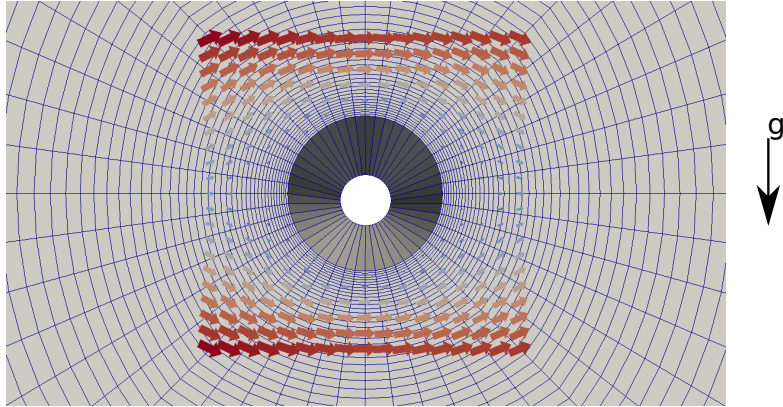


Figure 5.15. Dry hydrogen - Vector plot around the wire - Exemplary plot

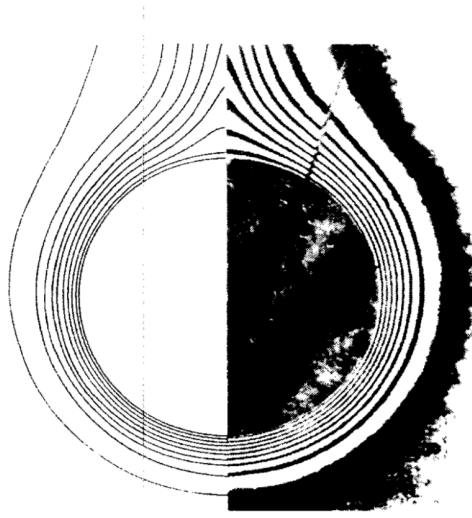


Figure 5.16. Natural convection around a cylinder at $Ra=10^5$ [White, 2006].

$5\mu m$ and dry hydrogen it is approximately $9 \cdot 10^{-3}$, which is very small compared to the situation shown Figure 5.16.

The just described situation of natural convection shall be compared with two cases at the hot wire:

- Highest free stream velocity
- Lowest free stream velocity

The expectation is, that natural convection can only occur in the low velocity case as the buoyant forces are dominated by the inertial forces at high velocities.

Therefore the results of Case 06-01 with 2 ms^{-1} inlet velocity is evaluated. This evaluation contains the temperature field and the vector plot in the previously shown area. Afterwards the same is evaluated for case 06-07 with 0.15 ms^{-1} inlet velocity.

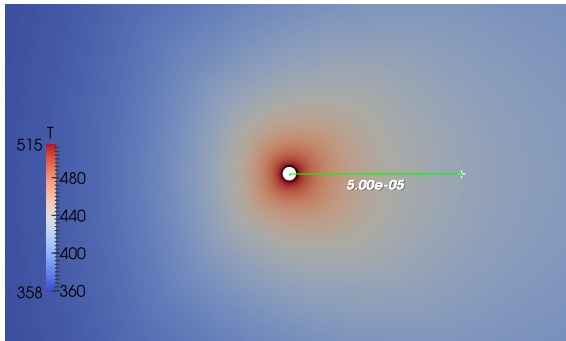


Figure 5.17. Dry hydrogen - Temperature distribution - highest velocity

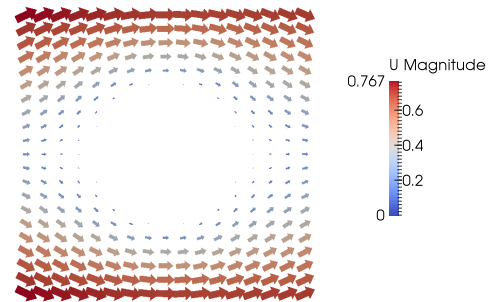


Figure 5.18. Dry hydrogen - Vector plot around the wire - highest velocity

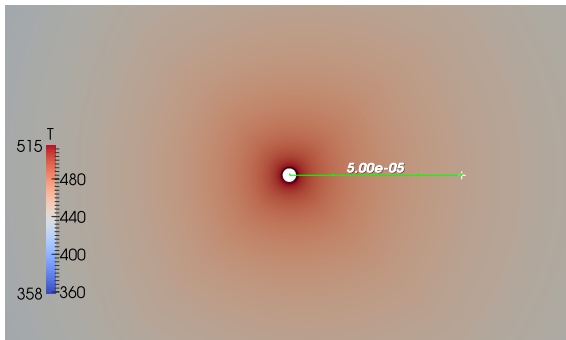


Figure 5.19. Dry hydrogen - Temperature distribution

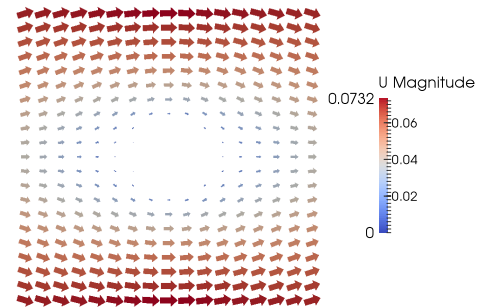


Figure 5.20. Dry hydrogen - Vector plot around the wire - lowest velocity

Comparing the temperature profiles in Figure 5.17 and in Figure 5.19 it can be seen that these profiles are very different: Due to the low velocity in Case 06-07, heat can diffuse better in all directions, than in Case 06-01, where most heat is transported to the outlet and the hot-zone is smaller than $5 \cdot 10^{-5} \text{m}$.

In Figure 5.18 and 5.20 it can be seen that the velocity vectors are following the shape of the wire: Coming from the left side, the flow has to change direction at the wire to flow around it. Thereby the flow direction is changed again behind the wire to proceed flowing from the left to the right.

Comparing all the figures it can be concluded that even the lowest free stream velocity is too high to see the effects of natural convection.

This chapter gave a detailed insight in the model, assuming critical operating points are the low velocity cases. It was shown, that the diffusion of heat upstream occurs always, but the distance upstream is small in all cases and becomes smaller with higher velocities. Related to this the approach of the film temperature was found to be a valid approach, because the thickness of the film temperature is in all cases smaller than 0.1 mm.

Last the unimportance of natural convection was shown with the help of vector plots. Even in the lowest free stream velocity cases, no natural convection was observed.

5.8 Nusselt number results

The Nusselt number is the main focus of this study, due to its importance for hot-wire anemometry, described in Chapter 1.2. At first overall Nusselt numbers of dry and humidified hydrogen are evaluated and linked with the Reynolds number at the wire.

To understand the heat flow from the wire to the surrounding better, local Nusselt numbers of dry hydrogen at different Reynolds numbers are compared.

5.8.1 Method of evaluation the Nusselt number

In Chapter 1.2 definitions for the Nusselt number are given in Equation 1.19 and Equation 1.20. The general way of calculating the Nusselt number was explained. It was discussed, that in order to estimate the convection coefficient " h " as well the heat flow needs to be known.

This heat flow can be determined on two ways:

1. A heat balance, relating inlet and outlet enthalpy streams using Equation 1.18
2. The OpenFOAM function "wallHeatFlux", giving the heat flow from the hot wire surface

These two methods must give the same results, otherwise the results might be disputable. Therefore the heat flows of simulations are evaluated with both methods and compared. The heat flows of the cases listed in Table 5.5 are evaluated. The comparison is done for the heat flow based on an OpenFOAM function "wallHeatFlux" and on the heat balance of the fluid, relating inlet and outlet temperature with the corresponding heat capacities there.

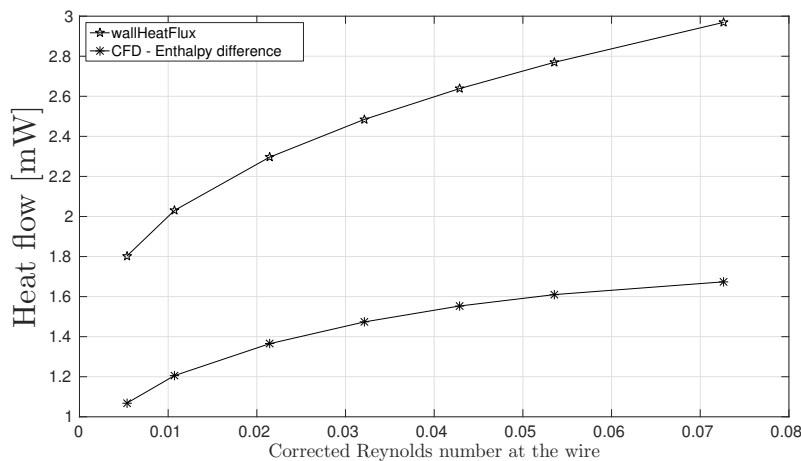


Figure 5.21. Dry hydrogen - Heat flow comparison [mW]

From Figure 5.21 the heat flow carried into the fluid can be seen. The two mentioned methods are compared and it can be observed that the heat flows are drastically different. With increasing Reynolds number at the wire, the curves tend to diverge more and more. The curve "CFD - Enthalpy difference" is based on Equation 1.18. As the temperature at the inlet is kept constant at 358.15 K, the potential error can only occur at the outlet where the temperature is evaluated based on the averaged temperature over the area with

the "patchAverage" function. The mass flow is calculated based on the velocity and the density at the inlet, which is as well assumed to be correct. Therefore this way of evaluating the heat flow may contain some inaccuracies due to the fact that material properties are needed, but it should give similar results as the other evaluation.

Case	Factor
06-01	1.77
06-02	1.72
06-03	1.70
06-04	1.69
06-05	1.68
06-06	1.68
06-07	1.69

Table 5.6. Dry hydrogen - Heat flow comparison.

Similar to Figure 5.21, Table 5.6 relates the two methods of evaluating the heat flow. Dividing Q_{wire} by $Q_{\text{Enthalpy difference}}$ gives the listed factors. The factors show again how big the difference between the two methods of evaluation is.

Case	Humidity	Factor
06-02	0%RH	1.72
06-02	20 %RH	0.97
06-02	40 %RH	1.11
06-02	60 %RH	1.00
06-02	80 %RH	1.05
06-02	100 %RH	1.13

Table 5.7. Humidified hydrogen - Heat flow comparison.

The same can be done for the cases of humidified hydrogen. These are listed in Table 5.7 and it can be seen that there are some variations, but only hydrogen with 0%RH (dry hydrogen) causes these drastic variations.

To determine the precise functionality of the function a lot of time is needed and several simulations have to be compared. As this is not the focus of this study, this is not done here.

Errors due to fluid properties can be excluded, as all simulations were carried out with the same data set of fluid properties.

Due to this and due to the previous explanation of the enthalpy based solution, it is decided to evaluate the Nusselt number based on the enthalpy difference of inlet and outlet.

5.8.2 Dry hydrogen

Berning and Shakshir [2015] showed that the power-law is the most accurate approach to calculate the Nusselt number of hot-wire anemometers in hydrogen streams. The formula was shown and explained in Equation 1.17. In case of calculating the Nusselt number, the Prandtl and Reynolds number and the coefficients are needed. Hilpert [1933] states that the Prandtl number is constant for gases of equal and constant composition and temperature. Furthermore the coefficient "n", related to the Prandtl number is usually set constant to "1/3". Hilpert [1933] carried out his study about heat transfer from pipes and wires to air with Reynolds numbers at the wire larger than 0.4. The results are thereby not directly usable for hot-wire anemometry, as the coefficients are unknown for the expected Reynolds number range. Therefore Equation 1.17 can be reformulated to the following expression:

$$\frac{Nu}{Pr^n} = C \cdot Re^m \quad (5.2)$$

With Equation 5.2 it is possible gain the missing coefficients using curve fits based on the power-law.

At first the overall Nusselt number from the CFD simulations is compared with the results from the laboratory. As mentioned before, the Reynolds numbers are corrected to achieve a better comparison of the curves. It may be noticed, that the correction factors for the CFD models are still 1.5 (Hagen-Poiseuille plate flow) but for results from the laboratory 2.0 (Hagen-Poiseuille pipe flow).

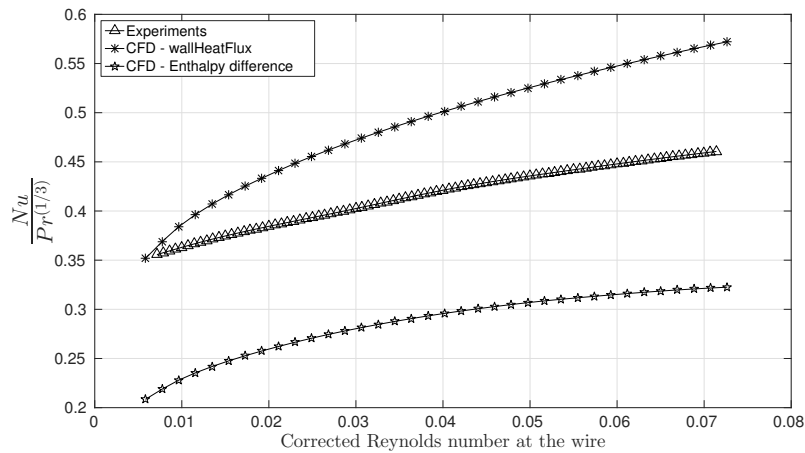


Figure 5.22. Dry hydrogen - Overall Nusselt number in comparison with laboratory results.

Figure 5.22 shows the curves of dry hydrogen based on CFD calculations, with both ways of evaluating the heat flow and the curve based on results from the laboratory.

Similar to Figure 5.21 the difference between the two methods can be observed. Furthermore the curve "CFD - Enthalpy difference" shows a larger distance to the laboratory results than the curve "CFD - Wire based". Following the assumption, that the curve "CFD - Enthalpy difference" is correct, it can be concluded that in the CFD simulations less heat is transferred to the fluid than in the laboratory. The following explanation could be a reason for this behavior:

The wire is hold in position with a holding mechanism, shown in Figure 4.2. As this

mechanism is connected to the wire, heat diffuses through the solid from the wire to the leads, keeping the wire in position. The leads are cooled down by the flow in the meantime. This additionally needed power may cause the higher heat flows and Nusselt numbers. However, to gain the coefficients needed for Equation 1.17 curve fits are done for the data of the curve "CFD - Enthalpy difference" and for the values from the experiments:

Coefficient	Value - CFD	Value - Experiments Velocity corrected with "2"	Value - Experiments uncorrected
C	0.5153	0.6169	0.6684
m	0.1749	0.1158	0.1158

Table 5.8. Power law coefficients dry hydrogen

Table 5.8 lists and compares different cases: At first the coefficients from the simulations are compared with corrected Reynolds number values from the laboratory. It can be seen from the Table that there are differences between the coefficients. This corresponds to the difference in the curves in Figure 5.22. To gain a better overview in correlation with previous publications, the results based on the uncorrected Reynolds numbers from Berning and Shakshir [2015] are shown as well. It can be seen, that only the factor "C" is affected by the correction. It acts as shift factor, whereupon the exponent "m" is unaffected by the correction. Therefore the more interesting coefficient is the exponent "m", which is still 0.0591 digits larger in the CFD results.

The coefficients were found using curve fits of the gained data. Next the corresponding figures are presented to estimate the accordance of the data to the power-law. The figures contain the data points gained from the simulations and from the laboratory and the fitted curve, respectively.

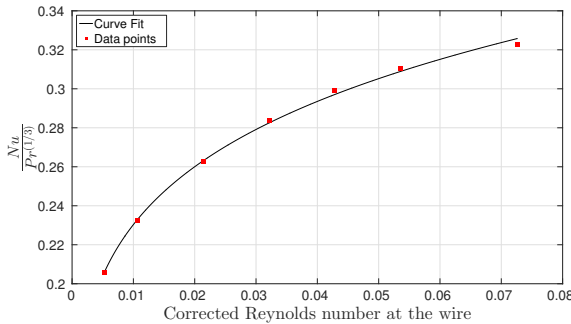


Figure 5.23. Dry hydrogen - Data points and curve fit - CFD simulations.

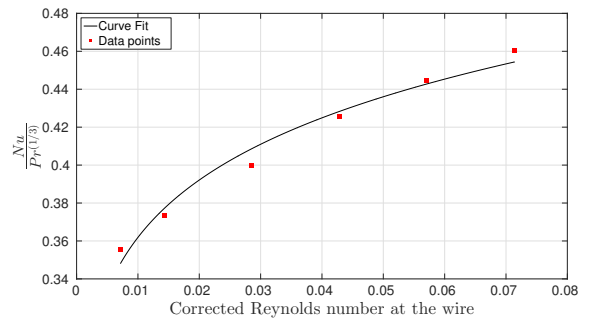


Figure 5.24. Dry hydrogen - Data points and curve fit - Experiments.

On the left, in Figure 5.23 it can be seen that the fitted curve fits the data points quite well. On the other side the corrected Reynolds number data from the laboratory are shown together with the curve corresponding curve fit. It can be seen, that the data from the laboratory show some variances, which might be caused by inaccuracies during the measurement.

5.8.3 Humidified hydrogen

The previous chapter contained the results of dry hydrogen with different free stream velocities. This chapter will deal with humidified hydrogen cases. Therefore three cases from Table 5.5 are chosen and simulated at 20%, 60%, 80% and 100% relative humidity (RH). The chosen cases are "06-02", "06-04" and "06-05".

Most interesting are the Nusselt number Reynolds number correlations. These are calculated based on the difference of enthalpy between the inlet and the outlet. The data from the simulation are used to create curve fits for the power-law, like for dry hydrogen.

The Figures 5.25, 5.26 and 5.27 contain the curve fits of five data points, starting from 0% RH at the lowest Reynolds number up to 100%RH at the highest Reynolds number. In Figure 5.25 it can be seen that the range of the Reynolds number starts at approximately 0.09 and ends at approximately 1.2.

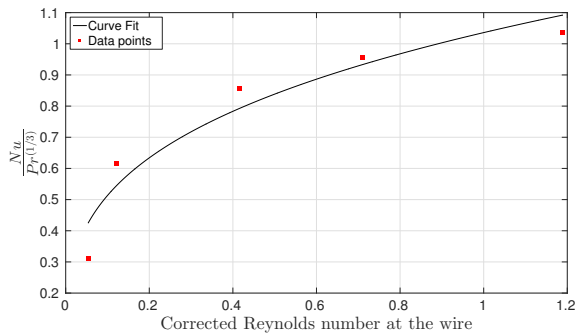


Figure 5.25. Humidified hydrogen - Case 06-02 - Curve fit

The other two figures, Figure 5.26 and Figure 5.27 already start at Reynolds numbers of approximately 0.03 and end at nearly 0.72 and 0.49, respectively.

The curves fit the data points not very precisely, but still with a R^2 of 0.9281 in Case 06-02, 0.948 in Case 06-04 and 0.9547 in Case 06-05.

Despite these variations, the curve fits are used to gain the coefficients needed for the power-law.

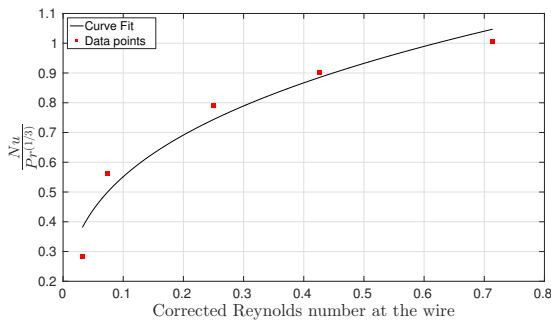


Figure 5.26. Humidified hydrogen - Case 06-04 - Curve fit

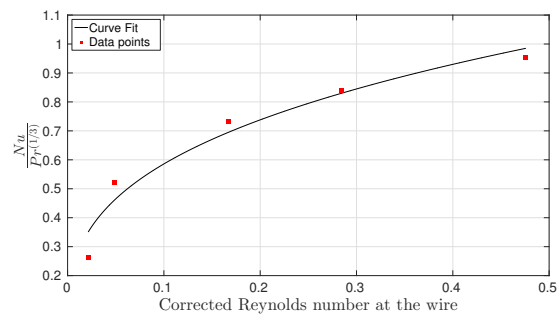


Figure 5.27. Humidified hydrogen - Case 06-05 - Curve fit

For a better overview, the data is plotted in one Figure 5.28 as smoothed curves. It can be seen, that all cases show the same tendency and that the data points are very close to each other. Although the initial Reynolds numbers of 0% RH are close together, the Reynolds numbers of 100% have higher distances to each other, when referring to Reynolds numbers.

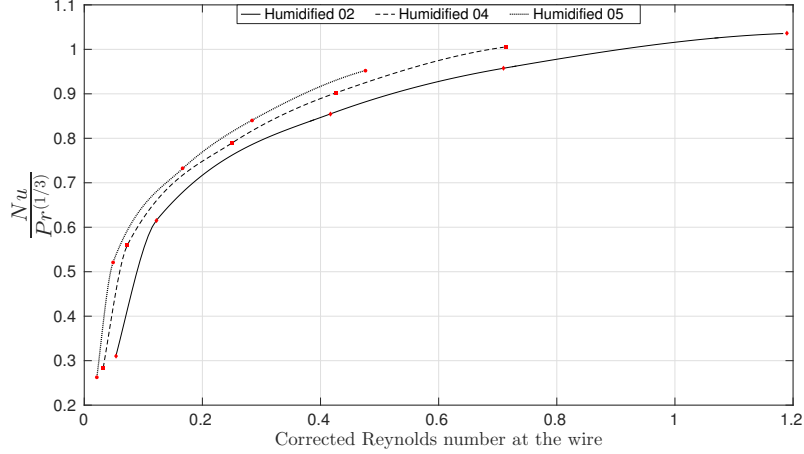


Figure 5.28. Humidified hydrogen - Comparison of the data

The coefficients are listed in Table 5.9. This table contains the already shown and listed coefficients of dry hydrogen, but as well all values from the humidified cases. Additionally the range of the Reynolds numbers is listed.

Parameter	CFD - Dry H_2	CFD - 06 02	CFD - 06 04	CFD - 06 05
C	0.6897	1.036	1.169	1.262
m	0.1753	0.3051	0.3262	0.3333
Re range	0.005 - 0.07	0.12 - 1.2	0.32 - 0.7	0.05 - 0.5

Table 5.9. Power law coefficients hydrogen - overall comparison

From the table a tendency can be observed: The factor "C" and the exponent "m" increase with an increasing Reynolds number. Shakshir et al. [2016a] have argued that a higher value for m will lead to a clearer reading of the relative hot wire signal that was termed E/E0 and is thus desirable.

Besides the shown results based on CFD simulations with humidified hydrogen, an experiment in the laboratory based on the same flow rates as the humidified case 06-02 was done. These results are shown in Figure 5.29.

The data is based on an experiment with a wire of $5\mu\text{m}$ in a pipe with 6 mm diameter, taking values at 0%, 20%, 60%, 80% and 100% RH. From Figure 5.29 it can be seen, that different than in the comparison of the dry hydrogen results, the values of the CFD simulation are higher than the experimental results. Taking Table 5.7 into account, it can be assumed that the CFD results are correct as both ways of evaluating the heat flow give similar results, except for the dry hydrogen point.

Excluding the first point, it can be concluded that more heat is transferred to the fluid in case of the two dimensional CFD simulation. This can be caused due to the difference of the two setups: In the CFD model, the wire experiences always the highest velocity. In the test setup the wire is hold in position by the leads. At first the wire does not experience an even velocity, as there is a velocity profile in the pipe. Secondly the leads might effect the flow as well.

Running a curve fit for the experimental data, "C" equals 0.767 and "m" equals 0.2309.

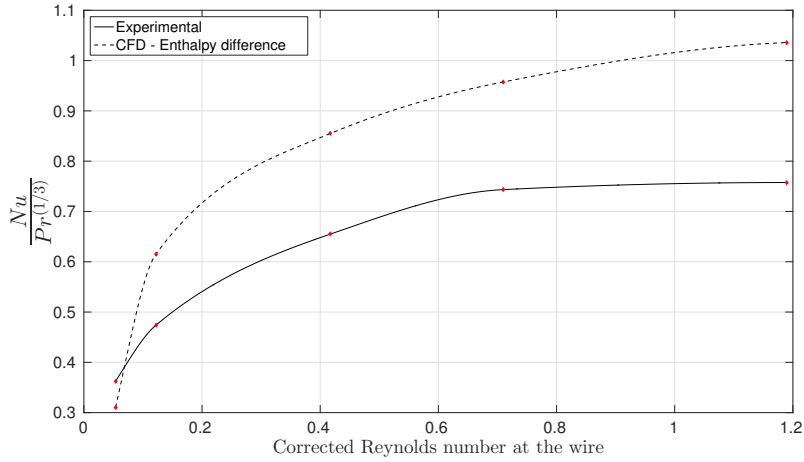


Figure 5.29. Humidified hydrogen - Case 06-02 - Comparison with experimental data

In this section the evaluation of the Nusselt number of dry and humidified hydrogen was presented. It was found that in case of dry hydrogen the values of the Nusselt number from the CFD simulation are smaller than the ones from the laboratory. This leads a bigger exponent "m" and to a slightly smaller "C". These data were fitted satisfyingly. The only unknown is still why there is a difference between the two ways of evaluating. The results of humidified hydrogen showed a different behavior: The CFD simulations result in higher Nusselt numbers than the experiments. It is unclear, if the results of dry hydrogen are more trustful than the ones of humidified hydrogen. As the difference between the evaluation methods is much higher in the dry hydrogen cases, it is assumed that these are inaccurate.

However, the results based on humidified hydrogen are fitted as well with the curve fits of the power law and show some deviations from the curve fit. Still the accuracy was found to be precise enough and coefficients were evaluated. These show, that both "C" and "m" increase with an increasing Reynolds number.

Furthermore a comparison of simulated and experimental data was done. Different than in the comparison between experimental and calculated results of dry hydrogen, it was found that in the CFD simulations more heat is transferred to the fluid than in the experiments.

5.8.4 Dry hydrogen - Local Nusselt number

In order to gain local heat flows the wire is split into four equal sized lateral areas. These are from now on called north, south, up(-stream) and down(-stream).

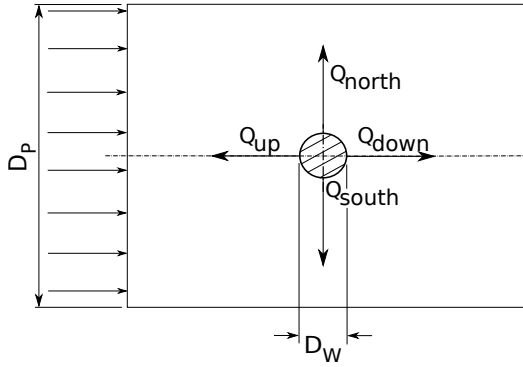


Figure 5.30. Illustration of the local Nusselt number.

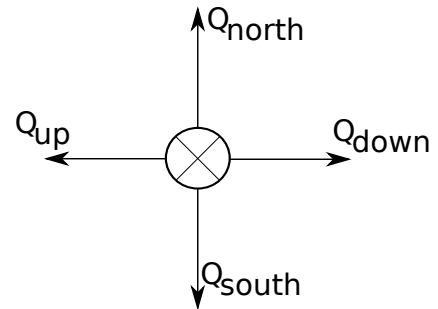


Figure 5.31. Wire subdivision.

The orientation of these areas and the related heat flows are visualized in Figure 5.30. To gain the heat flows from the four given directions, the wire surface is split into four areas, based on the schema shown in Figure 5.31. Based on this the local Nusselt numbers for different mass flows are evaluated. In Chapter 5.8.1 the ways of evaluating the heat flow were explained. To gain the local Nusselt number, local heat flows are needed which did not leave another opportunity than using the OpenFOAM function "wallHeatFlux". Thereby the shown results in this chapter can only be used to study the heat transfer generally. It has to be kept in mind that the numbers of the Nusselt number are probably too high.

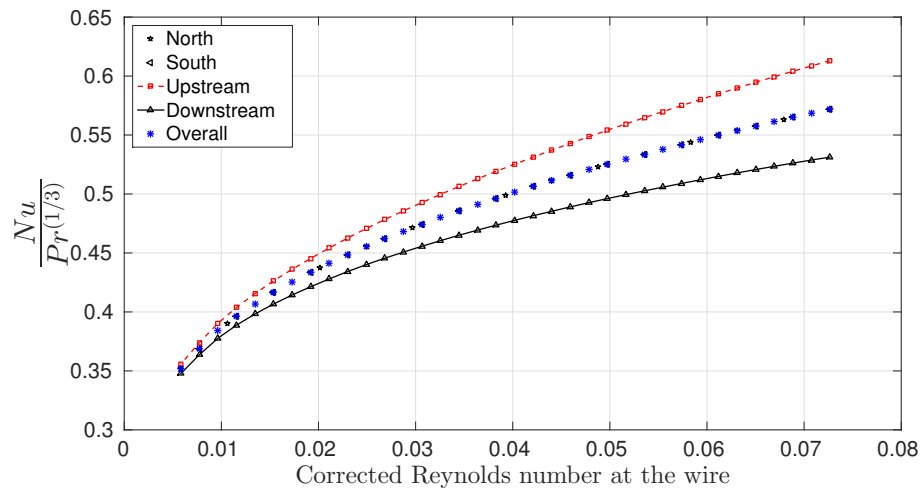


Figure 5.32. Dry hydrogen - Local Nusselt number.

The presented curves in Figure 5.32 show the Nusselt number divided by the Prandtl number to the power of 1/3 related with the corrected Reynolds number at the wire. The reasons for a correction of the Reynolds number and the way of doing it were explained in Chapter 3.1. Exemplary velocity profiles may be found in Chapter 5.5.

However, the presented figure shows total five curves, from which the curves of the north and south side are nearly identically with the overall Nusselt number curve. It is significantly that with decreasing Reynolds number, the local Nusselt numbers tend

to converge towards one value. This can be explained with the definition of the Nusselt number: As this dimensionless number relates convective and conductive heat transfer, the convective part decreases with decreasing Reynolds number. With smaller velocities the differences in convective heat transfer between north, south, up- and downstream become smaller as the flow regime approaches more and more the lower part of the flow regime of creeping flow or no flow at all. Of course this is limited by some natural convection that will occur at some point.

The main conclusion from this figure is where heat transfer takes place most: As the local Nusselt numbers upstream are highest, it is clear that that the heat transfer is highest here. Similar, heat transfer is lowest downstream as the local Nusselt number is lowest there.

5.9 Different wire diameter

The main focus of this study lays on the two dimensional model with a wire of $5 \mu\text{m}$ diameter. Besides this wire diameter, a $70 \mu\text{m}$ wire can be used as well in the laboratory. To evaluate the tendencies and gain general data of this case, a two dimensional model equal to the described one in Chapter 5 is set up. Instead of a $5 \mu\text{m}$ wire a $70 \mu\text{m}$ wire is used and the mesh is adopted to it.

A humidified curve based on the initial conditions of Case 06-02 is simulated. The resulting curve contains data points of 0%, 60%, 80% and 100% RH. To gain knowledge about the influence of the wire size, the results of the $70\mu\text{m}$ wire are compared with the already shown results of the $5\mu\text{m}$ wire.

Figure 5.33 shows the data points and the curve fit calculated with the $5\mu\text{m}$ wire. Next to it, based on the same conditions the data points and the curve fit simulated with the $70\mu\text{m}$ wire are shown in Figure 5.34.

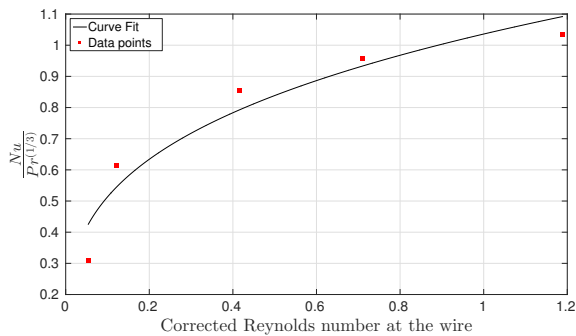


Figure 5.33. Humidified hydrogen - $5\mu\text{m}$ wire- Curve fit

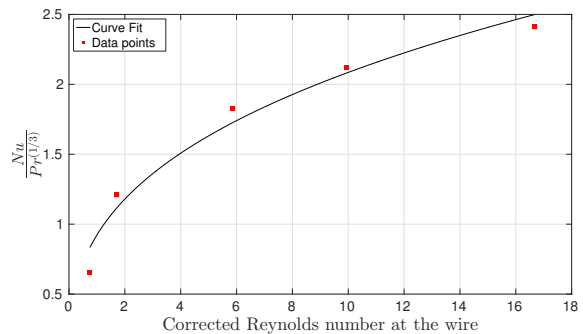


Figure 5.34. Humidified hydrogen - $70\mu\text{m}$ wire- Curve fit

From the Figures it can be seen that the Reynolds numbers of the μm wire are 14 times larger than the ones of the $5\mu\text{m}$ wire. This is due to the fact that the wire diameter of the $70\mu\text{m}$ wire is 14 times larger than the $5\mu\text{m}$ wire.

Furthermore the values on the y-axis are approximately twice as high in case of the $70\mu\text{m}$ wire compared with the $5\mu\text{m}$ wire.

Parameter	CFD	CFD	Lab. [Shakshir et al., 2016b]	Lab. Hilpert [1933]
Wire size	5 μm	70 μm	70 μm	Averaged
C	1.036	0.9227	1.34	0.821
m	0.3051	0.3541	0.224	0.385
Re range	0.12 - 1.2	0.75 - 16.7	0.2 - 4.5	1 - 40

Table 5.10. Power law coefficients - 70 μm wire

Table 5.10 lists the coefficients for the CFD simulations done with the 5 and 70 μm wire, the experimental results based on the 70 μm wire and additionally the coefficients from the experiments done by Hilpert [1933] based on air. Comparing the CFD results of the 70 μm wire with the experimental results from Hilpert [1933] and Shakshir et al. [2016b] it can be seen that the factor "C" of the CFD results is in between the other two results. The same is valid for the exponent "m".

The difference between the coefficients can be caused by the way of evaluating the data: Shakshir et al. [2016b] conducted tests in a smaller Reynolds number range, but used more data points, with several points between approximately $0.5 \leq \text{Re} \leq 1.5$. The data used to gain coefficients based on the CFD simulations cover a very wide Reynolds number range. Furthermore there is only one data point below Re 5, what lays the focus of the curve fit on the higher Reynolds number range. Besides this it is unknown how many data points Hilpert [1933] took into account.

Comparing only the results of the CFD simulations, it can be seen that with a larger wire diameter the coefficient "C" decreases and the exponent "m" increases.

3D model 6

Based on the same boundary conditions, listed in Table 5.3 a three dimensional model is created. This model shall be used to gain knowledge about the error that is made by choosing a 2D model for majority of the simulations. Although the three dimensional domain contains the original size of the $5\mu m$ wire, there is an important simplification: In the laboratory, the wire is kept in position by the leads. These are not only used to position the wire, but as well to achieve power supply. These are not included in the three dimensional domain, as they would increase the demand for computational cost. The three dimensional case ran on a computer with 8 processors, 16GB of RAM and it took approximately 100000 iterations until convergence could be assumed. This process took 17 days of computation time.

6.1 Model setup

The setup of the domain is referred to Figure 4.3. The meshing is created automatically with the tools blockMesh and snappyHexMesh based on geometry files. A brief process of the meshing process is given in Appendix C.2.

Parameter	Value	Unit
Pipe length (up to the wire center)	60	mm
Pipe diameter	6	mm
Wire length	1.25	mm
Wire diameter	$5 \cdot 10^{-3}$	mm
Number of cells	1830280	-
Refinement layers around the wire	5	-

Table 6.1. Three dimensional model - Parameter.

Table 6.1 lists the dimensions and number of cells of the three dimensional model. It can be seen that although the three dimensional domain is shorter than the two dimensional one, the number of cells is several times larger. The amount of computational power to solve the three dimensional model supports the statement of using two dimensional models for most of this study.

In order develop an efficient mesh, the cell size decreases towards the center of the pipe in longitudinal and radial direction. This can be seen in Figure 6.1, where the outlet of the pipe is shown. As the wire is placed in the center of the pipe, the cells have to decrease in size. Furthermore a refinement close to the pipe wall can be seen. The meshing process can be very stiff. Due to this it was prioritized to mesh the wire properly, including mesh layers around it. It would have been a mesh of higher quality, if the pipe had mesh layers close to the wall too, but in these cases the surface mesh of the wire was of very poor

quality.

Next the surface mesh of the wire is shown in Figure 6.2.

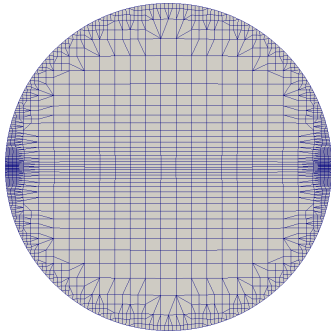


Figure 6.1. 3D Model - Surface mesh at the outlet.

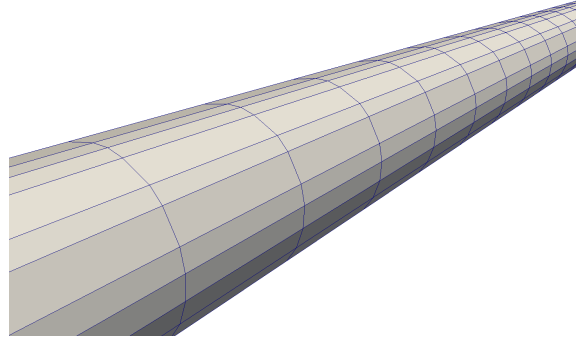


Figure 6.2. 3D Model - Surface mesh of the wire.

It can be seen, that the mesh looks smooth, although the number of cells is not very high. In Figure 6.3 the edge of one end of wire is shown. This is one of the most critical points during the meshing process with snappyHexMesh. Still it can be seen, that the edge is meshed correctly and that the mesh looks good.

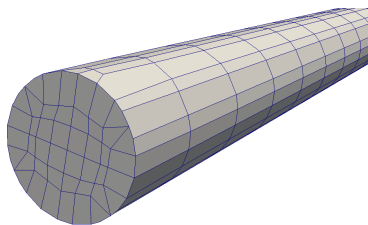


Figure 6.3. 3D Model - Surface mesh of the wire at its end.

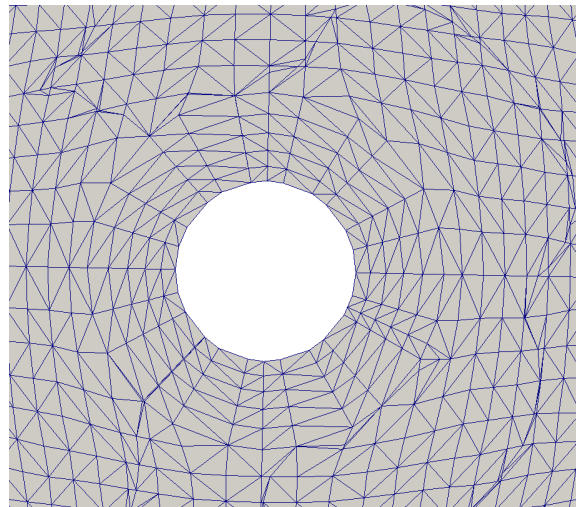


Figure 6.4. 3D Model - Volume mesh around the wire with local refinement layers.

Last the refinement around the wire is shown in Figure 6.4. From the figure the five refinement layers can be seen. It may be noticed that the appearance of the mesh is due to the way of representing the volume mesh: During the meshing process, the mesher moves cells as well along the wire axis. To enable a good representation, this is compensated by the post processing software (paraFoam).

6.2 Results

The three dimensional model is used to estimate the difference between the two dimensional model and real pipe flow. Its setup was described previously in Chapter 6.1. The first comparison was done based on case 06-02 with hydrogen at 20% RH. Following points will be evaluated in this chapter:

- Heat flow and Nusselt number
- Temperature profile 1 cm behind the wire
- Velocity profile 1 cm behind the wire

	2D model	3D model	Percentage difference
Heat flow [W m^{-1}]	45.728	41.868	9.2 %
Nusselt number	0.451	0.413	9.2 %

Table 6.2. 3D model - Heat evaluation.

Table 6.2 lists the heat flow per unit length of the wire and the Nusselt number of both models. It can be seen, that all values are lower in case of the 3D model. This supports the theory that at least in such simplified models, less heat is transferred from the wire to the fluid in pipe flow due to the velocity profile. In the two dimensional cases, the wire experiences always the maximal flow velocity, which results in a higher heat transfer rate.

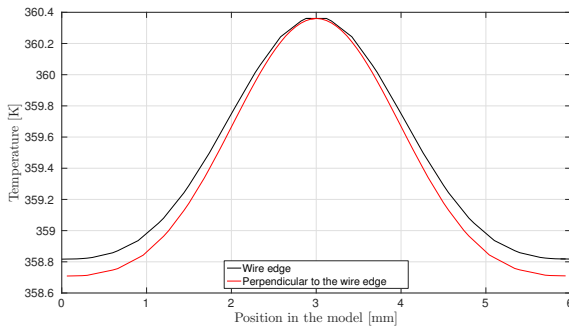


Figure 6.5. 3D model - Temperature profile

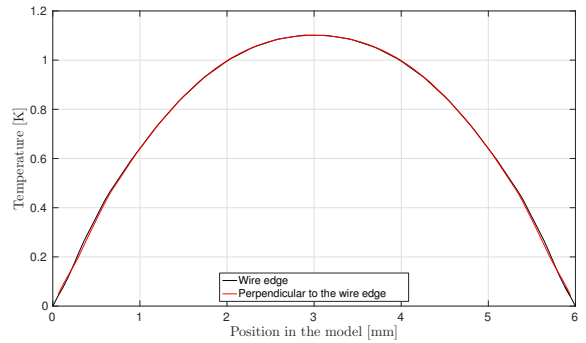


Figure 6.6. 3D model - Velocity profile

The profiles of temperature and velocity are shown in Figure 6.5 and 6.6. Both contain a curve for data taken from the edge of the wire in flow direction and one normal to that edge.

Figure 6.6 shows the velocity profiles and it can be seen, that the maximal velocity fits the Hagen-Poiseuille correlation for laminar pipe flow (the average inlet velocity is 0.57792 ms^{-1}). Furthermore no significant difference between the curves can be observed.

Different than the velocity profiles, the temperature profiles are not similar. The temperature in the edge of the wire is higher, than the temperature normal to the wire edge. It can be seen, that close to the pipe wall the temperature is approximately 0.5 K higher than the inlet temperature.

Last two plots in the longitudinal edge of the wire shall give an overview of the temperature and the velocity.

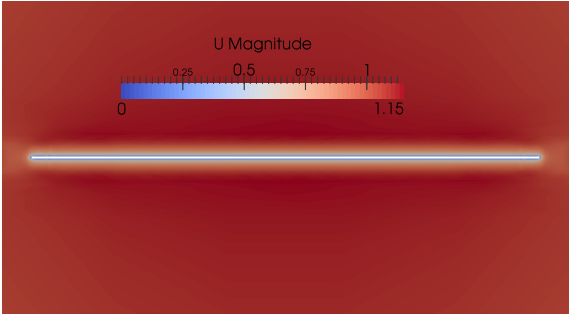


Figure 6.7. 3D model - Velocity field around the wire

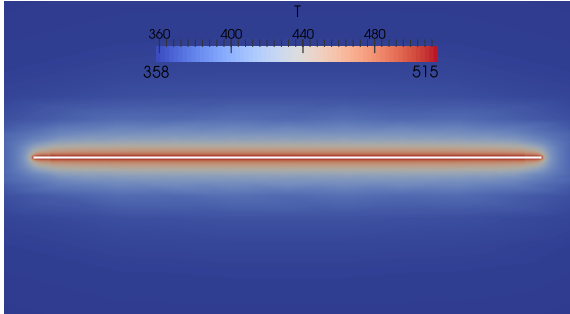


Figure 6.8. 3D model - Temperature field around the wire

Although the data in Table 6.2 indicate that there is a difference between the two and three dimensional case, from Figure 6.7 and Figure 6.8 it can be concluded, that the influence of the velocity profile is very small as it cannot be seen from the presented figure.

From this chapter it can be concluded, that the heat transfer of the two dimensional model is higher compared with a three dimensional one. This has to be kept in mind, as the results of this study are based on two dimensional models.

This study had the aim to build a model of a hot wire to gain knowledge of the influence of this wire to its surrounding and to evaluate overall and local Nusselt numbers. In this Chapter the results will be summed up and discussed.

7.1 Influence on the surrounding

At first it was found that the velocities upstream of the wire in the domain center fit the Hagen-Poiseuille correlation of $u_{max} = 1.5 \cdot u_{av}$ for laminar flow between two parallel and not moving plates.

A strong dependency of the outlet temperature to the flow velocity was found: Increasing the velocity from very low regimes, the outlet temperature decreases very strong. Proceeding results in an exponential curve that will come closer to the inlet temperature but will never reach it.

Besides the outlet temperature, the heat diffusion was of interest. By using the Peclet number, based on the pipe diameter and extracting the temperature along the center line, it could be concluded that heat diffuses upstream, but less than approximately 0.2 cm.

One of the main questions was if the film temperature is still correct in cases of very low velocities. Thereupon the thickness of the film temperature at the wire was elucidated. Even in the case with the lowest velocity, the film temperature layer was thinner than approximately 0.1 mm. Due to this the approach of the film temperature is assumed to be correct for the presented cases.

Last the influence of natural convection could be neglected in all presented cases.

7.2 Nusselt number and estimation of the coefficients

To gain Nusselt numbers dependent on the Reynolds number several simulations with dry and humidified hydrogen were conducted. They all had in common, that the inlet temperature was kept constant at 85°C and that the fluid properties were identical for each relative humidification, respectively.

During the evaluation of the overall Nusselt numbers, an inconsistency was found: The OpenFOAM internal function "wallHeatFlux" did not always equal the heat flow calculated based on the first law of thermodynamics. This applies especially for the dry hydrogen cases, where factors of nearly 1.7 were found. In case of humidified hydrogen this difference could not be observed.

A third way of calculating the Nusselt number based on the temperature gradient close to the wall was shown, but not compared to the other two ways.

However, as it was not the main focus of this study to evaluate the OpenFOAM function, the results of study are evaluated based on the first law of thermodynamics. Comparing

the results of the CFD simulations with the $5\mu\text{m}$ wire to experimental data two main conclusions could be found:

1. In case of dry hydrogen, more heat is transferred from the wire to the fluid during the experiments than in the CFD simulation
2. In case of humidified hydrogen the exact opposite was found: In the CFD simulations more heat was transferred to the fluid than in the experiment

Based on these results the coefficients for the power law where found:

- Dry hydrogen: $C=0.5153$ and $m=0.1749$
- Humidified hydrogen $1.036 \leq C \leq 1.262$ and $0.3051 \leq m \leq 1/3$

These coefficients are dependent on the Reynolds number. In case of humidified hydrogen for example, the coefficients increase both with increasing Reynolds number.

Furthermore the local Nusselt numbers of dry hydrogen were evaluated and it was found that most heat (high Nusselt number) is transferred from the wall upstream and least from the wall downstream of the wire. The Nusselt numbers north and south from the wire equal the average Nusselt number.

All discussed results where conducted based on a $5\mu\text{m}$ wire. As a $70\mu\text{m}$ wire is also used in the laboratory, a humidified curve with a $70\mu\text{m}$ wire was simulated. Due to the larger diameter of the wire, the Reynolds numbers were high enough to compare the coefficients with experimental data from Hilpert [1933] and Shakshir et al. [2016b]. Both coefficients lay in between the coefficients from the mentioned sources. C equals 0.9227 and m equals 0.3541.

The presented results are all gained from a two dimensional model where the wire experiences always the maximal velocity. To estimate the difference to a three dimensional model, one point from a humidified curve was calculated three dimensional. Due to the different inflow, less heat per wire length is transferred to the fluid. Thereby the Nusselt number was nearly 9% lower.

Future work

8

Several challenges were faced which have to be evaluated more precisely. At first the difference between the "wallHeatFlux" function and the heat flow based on enthalpy streams needs to be evaluated. As OpenFOAM saves only pressure, temperature and velocity fields, the first step could be to rewrite the solver in a way that the material properties density, thermal conductivity, heat capacity and viscosity are saved with each write step. If these show physical behavior, the same should be done for the enthalpy field to evaluate enthalpy streams directly without an averaged temperature. Furthermore the "wallHeatFlux" function itself could be evaluated by studying the code.

However, another important approach could be to evaluate the accuracy of OpenFOAM by running some simulations with the same mesh and the same boundary conditions in another (commercial) software, like Ansys Fluent or Ansys CFX for example.

More important than a software comparison is a very critical assumption: The surface temperature of the wire is set constant in all simulations and assumed to be constant in the experiments. From basic thermodynamics it is known, that such a situation does not exist. It is thereby recommended to evaluate if the temperature profile in the wire is so small that the assumption of constant temperature is valid or if it creates a drastic error. If OpenFOAM is considered to run the simulation, "chtMultiRegionSimpleFoam" is a solver that is capable of running such a case.

This model could be build up even more complex and thereby more accurate by using the multiphysics software COMSOL. It should contain the already described conjugate heat transfer from the solid wire to the fluid, but as well an ohmic heating term for the wire. Including ohmic heating, it is possible to relate not only fluid properties to the temperature but as well the solid properties like the resistance for example.

Bibliography

- Abid and Masoud, 2013.** Rabbani Abid and Rokni Masoud. *Effect of nitrogen crossover on purging strategy in PEM fuel cell systems*. Applied Energy, 2013.
- Berning, 2012.** Torsten Berning. *The dew point temperature as a creterion for optimizing the operating conditions of proton exchange membrane fuel cells*. International Journal of Hydrogen Energy, 2012.
- Berning, 2013.** Torsten Berning. *A method for the ad hoc and real-time determination of the water balance in a PEMFC*. International Journal of Hydrogen Energy, 2013.
- Berning, 2011.** Torsten Berning. *On water transport in polymer electrolyte membranes during the passage of current*. International Journal of Hydrogen Energy, 2011.
- Berning and Shakshir, 2015.** Torsten Berning and Saher Al Shakshir. *Applying hot wire anemometry to directly measure the water balance in a proton exchange membrane fuel cell - Part 1:Theory*. Hydrogen Energy Publications, 2015.
- CFD-Online, a.** CFD-Online. *fixedFluxpressure*.
<http://www.cfd-online.com/Forums/openfoam-solving/82581-i-need-explanations-about-fixedfluxpressure.html>. Accessed: 2016-05-29.
- CFD-Online, b.** CFD-Online. *Temperature gradient at the wall*. <http://www.cfd-online.com/Forums/openfoam/65701-temperature-gradient-wall.html>. Accessed: 2016-05-21.
- Comsol-Multiphysics-Cyclopedia.** Comsol-Multiphysics-Cyclopedia. *The Boussinesq Approximation*.
<https://www.comsol.com/multiphysics/boussinesq-approximation>. Accessed: 2016-05-26.
- ERCOFTAC, 2000.** ERCOFTAC. *Special Interest Group on "Quality and Trust in Industrial CFD" Best Practice Guidelines*. Handbook. European Research Community On Flow, Turbulence And Combustion, 2000.
- FuelCellToday.** FuelCellToday. *PEMFC*.
<http://www.fuelcelltoday.com/technologies/pemfc>. Accessed: 2016-02-18.
- Haeri and Shrimpton, 2013.** S. Haeri and J.S. Shrimpton. *A correlation for the calculation of the local Nusselt number around circular cylinders in the range $10 < Re < 250$ and $0.1 < Pr < 40$* . International Journal of Heat and Mass Transfer, 2013.
- Hayre, Cha, Colella, and Prinz, 2006.** Ryan P. O Hayre, Suk-Won Cha, Whitney Colella, and Fritz B. Prinz. *Fuel Cell Fundamentals*. Handbook. John Wiley and Sons, 2006.

- Hilpert, 1933.** R. Hilpert. *Wärmeabgabe von geheizten Drähten und Rohren im Luftstrom*. VDI Danzig Langfuhr, 1933.
- Horacio J., Santiago Márquez, Juan M., and Norberto M., 2013.** Aguerre Horacio J., Damián Santiago Márquez, Gimenez Juan M., and Nigro Norberto M. *Modeling of compressible fluid problems with OpenFOAM using dynamic mesh technology*. Mecánica Computacional Vol XXXII, 2013.
- Jansen and Overvelde, 2001.** G.J.M. Jansen and M.L.J. Overvelde. *Water transport in the proton-exchange-membrane fuel cell measurements of the effective drag coefficient*. Journal of Power Sources, 2001.
- Kumar and Mittal, 2004.** Bhaskar Kumar and Sanjay Mittal. *Prediction of the critical Reynolds number flow past a circular cylinder*. Computer methods in applied mechanics and engineering, 2004.
- Lomas, 1986.** C. G Lomas. *Fundamentals of Hot Wire Anemometry*. Handbook. Cambridge University Press, 1986.
- OpenFOAM, a.** OpenFOAM. *BuoyantBoussinesqPisoFoam*. <https://openfoamwiki.net/index.php/BuoyantBoussinesqPisoFoam>. Accessed: 2016-02-01.
- OpenFOAM, b.** OpenFOAM. *BlockMesh*. <http://cfd.direct/openfoam/user-guide/blockmesh/>. Accessed: 2016-03-01.
- Peighambardoust, S.Rowshanzamir, and M.Amjadi, 2010.** S.J. Peighambardoust, S.Rowshanzamir, and M.Amjadi. *Review of the proton exchange membranes for fuel cell applications*. 2010.
- Schlichting and Gersten, 2014.** Herrmann Schlichting and Klaus Gersten. *Boundary Layer Theory*. ISBN: 978-81-8128-121-0, Handbook. Springer Verlag, 2014.
- Shakshir, Andreasen, and Berning, 2016a.** Saher Al Shakshir, Søren Juhl Andreasen, and Torsten Berning. *Applying hot-wire anemometry to directly measure the water balance in a proton exchange membrane fuel cell - Part 2: Experimental*. XX, 2016.
- Shakshir, Hussain, and Berning, 2016b.** Saher Al Shakshir, N. Hussain, and Torsten Berning. *Employing Hot Wire Anemometry to Directly Measure the Water Balance in a Proton Exchange Membrane Fuel Cell*. The First Pacific Rim Thermal Engineering Conference, 2016.
- Subramanian.** R.Shankar Subramanian. *Heat transfer to or from a fluid flowing through a tube*. Clarkson University.
- VDI, 2010.** VDI. *VDI Heat Atlas, Second Edition*. ISBN: 978-3-540-77876-9, Handbook. VDI-Verlag GmbH, Düsseldorf, 2010.
- White, 2006.** Frank M. White. *Viscous Fluid Flow*. ISBN: 007-124493-X, Handbook. McGrawHil, 2006.

Wilke, 1950. C. R. Wilke. *A Viscosity Equation for Gas Mixtures*. The Journal of Chemical Physics, 18(4), 1950.

Z.Sharaf and F.Orhan, 2014. Omar Z.Sharaf and Mehmet F.Orhan. *An overview of fuel cell technology: Fundamentals and applications*. 2014.

Material properties

A

A.1 Raw data

This part of the Appendix contains the data of dry hydrogen and water vapor, which was used to gain the functions of different material properties, depended on temperature.

A.1.1 Hydrogen

T [K]	ρ [kg m ⁻³]	C_p [J kg ⁻¹ K ⁻¹]	μ [Ns m ⁻²]	k [W m ⁻¹ K ⁻¹]
273.15	0.08995	13920	$8.39 \cdot 10^{-6}$	0.1652
323.15	0.076306	14349	$9.43 \cdot 10^{-6}$	0.1881
373.15	0.06584	14473	$1.04 \cdot 10^{-5}$	0.2095
423.15	0.05806	14492	$1.14 \cdot 10^{-5}$	0.02296
473.15	0.05193	14482	$1.23 \cdot 10^{-5}$	0.2486
573.15	0.0424	14540	$1.38 \cdot 10^{-5}$	0.294
673.15	0.0362	14590	$1.54 \cdot 10^{-5}$	0.332

Table A.1. Hydrogen.

A.1.2 Water vapor

T [K]	ρ [kg m ⁻³]	C_p [J kg ⁻¹ K ⁻¹]	μ [Ns m ⁻²]	k [W m ⁻¹ K ⁻¹]
273.15	0.80380	1874	$8.956 \cdot 10^{-6}$	0.01673
323.15	0.67940	1874	$1.078 \cdot 10^{-5}$	0.02032
373.15	0.58840	1880	$1.265 \cdot 10^{-5}$	0.02429
423.15	0.51890	1908	$1.456 \cdot 10^{-5}$	0.02861
473.15	0.46400	1935	$1.650 \cdot 10^{-5}$	0.03326
573.15	0.38310	1997	$2.045 \cdot 10^{-5}$	0.04345
673.15	0.32620	2066	$2.446 \cdot 10^{-5}$	0.05467

Table A.2. Water vapor.

A.2 Functions

This Chapter contains the functions for hydrogen with following relative humidities:

- 0% RH
- 20% RH
- 40% RH
- 60% RH
- 80% RH
- 100% RH

A.2.1 H2 0% RH

Function	Unit		T	T ²	T ³	T ⁴
$\rho(T)$	[kg m ⁻³]	0.2279	-7.589 · 10 ⁻⁴	1.082 · 10 ⁻⁶	5.606 · 10 ⁻¹⁰	0
$C_p(T)$	[J kg ⁻¹ K ⁻¹]	9386	37.42	-0.1025	1.242 · 10 ⁻⁴	-5.555 · 10 ⁻⁸
$\mu(T)$	[N s m ⁻²]	1.98 · 10 ⁻⁶	2.601 · 10 ⁻⁸	-9.145 · 10 ⁻¹²	0	0
$k(T)$	[W m ⁻¹ K ⁻¹]	4.287 · 10 ⁻²	4.602 · 10 ⁻⁴	-4.39 · 10 ⁻⁸	0	0

Table A.3. Coefficients for hydrogen 0% RH.

A.2.2 H2 20% RH

Function	Unit		T	T ²	T ³	T ⁴
$\rho(T)$	[kg m ⁻³]	1.116	-3.794 · 10 ⁻³	5.525 · 10 ⁻⁶	-2.921 · 10 ⁻⁹	0
$C_p(T)$	[J kg ⁻¹ K ⁻¹]	6315	14.65	-3.831 · 10 ⁻²	4.507 · 10 ⁻⁵	-1.943 · 10 ⁸
$\mu(T)$	[N s m ⁻²]	1.245 · 10 ⁻⁶	2.219 · 10 ⁻⁸	-7.157 · 10 ⁻¹²	0	0
$k(T)$	[W m ⁻¹ K ⁻¹]	3.186 · 10 ⁻²	4.224 · 10 ⁻⁴	-5.592 · 10 ⁻⁸	0	0

Table A.4. Coefficients for hydrogen 20% RH.

A.2.3 H2 40% RH

Function	Unit		T	T ²	T ³	T ⁴
$\rho(T)$	[kg m ⁻³]	1.473	-5.013 · 10 ⁻³	7.311 · 10 ⁻⁶	-3.869 · 10 ⁻⁹	0
$C_p(T)$	[J kg ⁻¹ K ⁻¹]	5283	3.593	-6.075 · 10 ⁻³	3.954 · 10 ⁻⁶	0
$\mu(T)$	[N s m ⁻²]	7.908 · 10 ⁻⁷	1.873 · 10 ⁻⁸	-5.506 · 10 ⁻¹²	0	0
$k(T)$	[W m ⁻¹ K ⁻¹]	2.327 · 10 ⁻²	3.779 · 10 ⁻⁴	-5.507 · 10 ⁻⁸	0	0

Table A.5. Coefficients for hydrogen 40% RH.

A.2.4 H2 60% RH

Function	Unit		T	T ²	T ³	T ⁴
$\rho(T)$	[kg m ⁻³]	2.067	-9.446 · 10 ⁻³	2.105 · 10 ⁻⁵	-2.292 · 10 ⁻⁸	9.758 · 10 ⁻¹²
$C_p(T)$	[J kg ⁻¹ K ⁻¹]	4295	1.684	-2.407 · 10 ⁻³	1.679 · 10 ⁻⁶	0
$\mu(T)$	[N s m ⁻²]	5.025 · 10 ⁻⁷	1.571 · 10 ⁻⁸	-4.178 · 10 ⁻¹²	0	0
$k(T)$	[W m ⁻¹ K ⁻¹]	2.689 · 10 ⁻²	2.865 · 10 ⁻⁴	0	0	0

Table A.6. Coefficients for hydrogen 60% RH.

A.2.5 H2 80% RH

Function	Unit		T	T ²	T ³	T ⁴
$\rho(T)$	[kg m ⁻³]	1.786	-6.083 · 10 ⁻³	8.877 · 10 ⁻⁶	-4.701 · 10 ⁻⁹	0
$C_p(T)$	[J kg ⁻¹ K ⁻¹]	3699	0.33	2.475 · 10 ⁻⁴	0	0
$\mu(T)$	[N s m ⁻²]	3.17 · 10 ⁻⁷	1.314 · 10 ⁻⁸	-3.135 · 10 ⁻¹²	0	0
$k(T)$	[W m ⁻¹ K ⁻¹]	1.987 · 10 ⁻²	2.518 · 10 ⁻⁴	0	0	0

Table A.7. Coefficients for hydrogen 80% RH.

A.2.6 H2 100% RH

Function	Unit		T	T ²	T ³	T ⁴
$\rho(T)$	[kg m ⁻³]	1.869	-6.365 · 10 ⁻³	9.29 · 10 ⁻⁶	-4.92 · 10 ⁻⁹	0
$C_p(T)$	[J kg ⁻¹ K ⁻¹]	3190	0.1216	4.488 · 10 ⁻⁴	0	0
$\mu(T)$	[N s m ⁻²]	1.963 · 10 ⁻⁷	1.1 · 10 ⁻⁸	-2.329 · 10 ⁻¹²	0	0
$k(T)$	[W m ⁻¹ K ⁻¹]	1.366 · 10 ⁻²	2.208 · 10 ⁻⁴	0	0	0

Table A.8. Coefficients for hydrogen 100% RH.

Blocking plan B

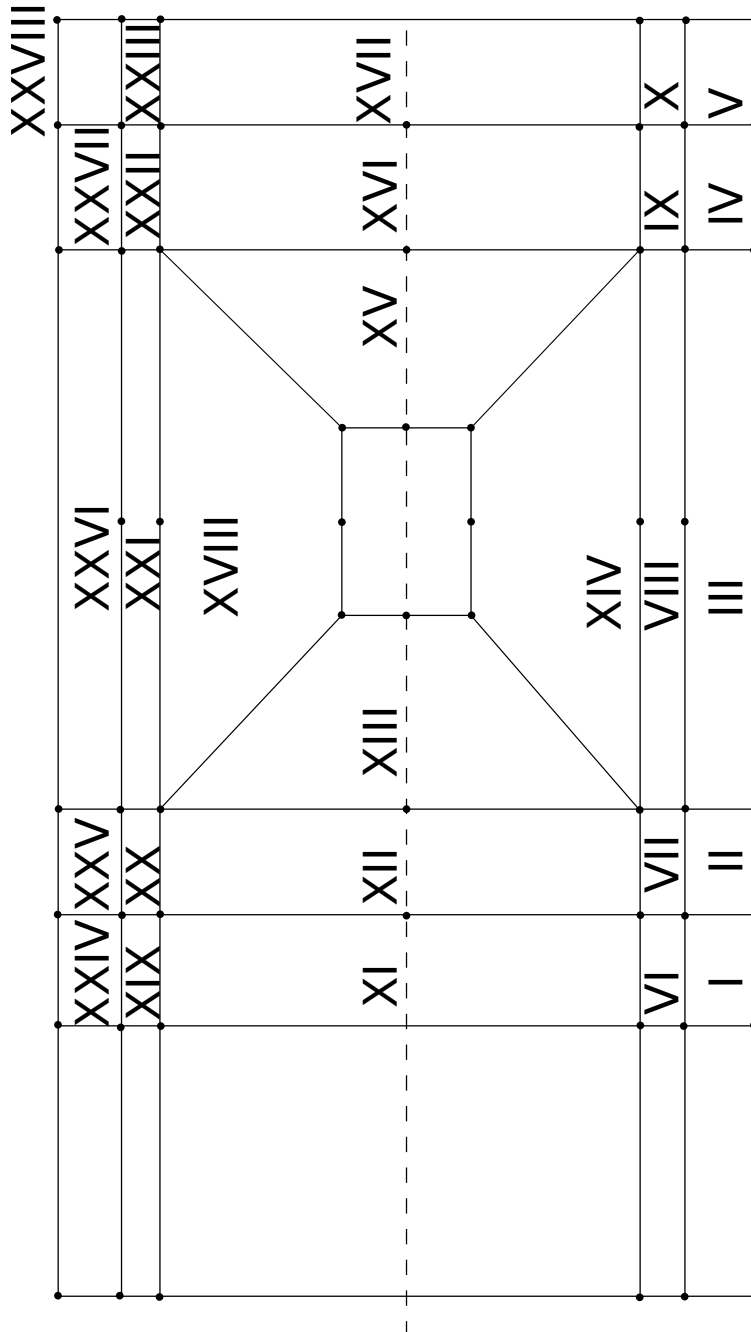


Figure B.1. Blocking plan.

Guideline for the enclosure



C.1 Content

The enclosure contents the following:

1. Two dimensional cases
2. The three dimensional case
3. An EXCEL file containing all results
4. The "wallGradT" shown in Appendix D

The following table lists the detailed content of the folder "Two-Dimensional". The first column contains the name of the folder which is already indicating the content: E.g. the folder "6mm-02-0-U-1-4744-0perc" is based on a pipe diameter of 6mm and the overall case number is "02" and the subdirectory is "0". These are the same case numbers, already used in the main report, like 06-02 e.g. This is followed by "U-1-4744" as the inlet velocity of 1.4744 ms^{-1} . Last the relative humidity is given by "0perc" standing for 0% RH.

To give a better overview, the wire diameter and the relative humidity are given as well in the table.

Folder name	Wire Diamter	RH	Folder name	Wire Diameter	RH
6mm-01-U-2-0-0perc	$5\mu\text{m}$	0%	6mm-05-0-U-0-5898-0perc	$5\mu\text{m}$	0%
6mm-02-0-U-1-4744-0perc	$5\mu\text{m}$	0%	6mm-05-1-U-0-23104-20perc	$5\mu\text{m}$	20%
6mm-02-1-U-0-577592-20perc	$5\mu\text{m}$	20%	6mm-05-2-U-0-27915-40perc	$5\mu\text{m}$	40%
6mm-02-2-U-0-69788-40perc	$5\mu\text{m}$	40%	6mm-05-3-U-0-36299-60perc	$5\mu\text{m}$	60%
6mm-02-3-U-0-90748-60perc	$5\mu\text{m}$	60%	6mm-05-4-U-0-47929-80perc	$5\mu\text{m}$	80%
6mm-02-4-U-1-19821-80perc	$5\mu\text{m}$	80%	6mm-05-5-U-0-64019-100perc	$5\mu\text{m}$	100%
6mm-02-5-U-1-60049-100perc	$5\mu\text{m}$	100%	6mm-06-U-0-29490perc	$5\mu\text{m}$	0%
6mm-03-U-1-1795-0perc	$5\mu\text{m}$	0%	6mm-07-U-0-1474perc	$5\mu\text{m}$	0%
6mm-04-0-U-0-8846-0perc	$5\mu\text{m}$	0%	6mm-100-U-1-4744-0perc	$70\mu\text{m}$	0%
6mm-04-1-U-0-346565-20perc	$5\mu\text{m}$	20%	6mm-101-U-0-577592-20perc	$70\mu\text{m}$	20%
6mm-04-2-U-0-54449-60perc	$5\mu\text{m}$	60%	6mm-102-U-0-90748-60perc	$70\mu\text{m}$	60%
6mm-04-3-U-0-71893-80perc	$5\mu\text{m}$	80%	6mm-103-U-1-19821-80perc	$70\mu\text{m}$	80%
6mm-04-4-U-0-96029-100perc	$5\mu\text{m}$	100%	6mm-104-U-1-60049-100perc	$70\mu\text{m}$	100%

Table C.1. Enclosure - Overview over cases.

C.2 How to run a case

To save space, the result and mesh files are not in the enclosure. If these are needed, following software is required:

- Python
- OpenFOAM 2.4.0
- paraFoam or paraview

Python is only needed to create the mesh of the two dimensional cases. Assuming the software is installed, the first step is to navigate into the wished folder. In all folders a file called `"run_meshing"` is placed. This can be executed by typing `./run_meshing` in the terminal.

The following commands are executed from this file for the two dimensional model:

- Run the python file `"wire_optimised.py"` to setup the `"blockMeshDict"` file
- Create the mesh with `"blockMesh"`
- Check the mesh quality with `"checkMesh -meshQuality"`

and for the three dimensional model:

- Create the background mesh with `"blockMesh"`
- Run `"surfaceFeatureExtract"`
- Prepare parallel computing `"decomposePar"`
- Run with eight cores `"mpirun -np 8 snappyHexMesh -overwrite -parallel"`
- Merge the mesh with `"reconstructParMesh -constant"`
- Check the mesh quality with `"checkMesh -meshQuality"`

It may be noticed that some commands are not listed. These are mainly used to create and delete folders that are needed in the meshing process.

After the meshing process is done, the simulation can be started with the command `"buoyantSimpleFoam"`. If parallel computing is wished, this can be done again, by `"decomposePar"` and `"mpirun -np XX buoyantSimpleFoam -parallel"`. Therefore it is necessary to adjust the number of cores in the file `"system/decomposeParDict"` to the wished number. This number has to equal the `"XX"` from the run command.

It is very important to keep in mind that these simulations need a high number of iterations to converge, dependent on the inlet velocity. Generally higher inlet velocities tend to converge faster than low velocities.

Furthermore the three dimensional model is not recommended to run, as it needs a high amount of computational power.

